

THESIS

PROCESSES CONTROLLING THE BEHAVIOR OF LNAPLS AT
GROUNDWATER SURFACE WATER INTERFACES

Submitted by

Alison M. Hawkins

Department of Civil and Environmental Engineering

In partial fulfillment of the requirements

For the Degree of Master of Science

Colorado State University

Fort Collins, Colorado

Spring 2013

Master's Committee:

Advisor: Tom Sale

Julio Zimbron

Michael Ronayne

Copyright by Alison Michelle Hawkins 2013

All Rights Reserved

ABSTRACT

PROCESSES CONTROLLING THE BEHAVIOR OF LNAPLS AT GROUNDWATER SURFACE WATER INTERFACES

Releases of Light Non-Aqueous Phase Liquids (LNAPLs) are a significant problem at many sites. This thesis explored governing processes pertaining to LNAPL releases at groundwater surface water interfaces (GSIs). Governing processes were investigated via laboratory studies and a preliminary analysis of forces controlling LNAPL occurrence in unsaturated media.

A total of six laboratory sand tank experiments were conducted using novel applications of fluorescing dyes. The results of these experiments provide unique insights regarding LNAPL behavior in porous media. Key insights include:

- LNAPLs occur in three distinct zones, herein referred to as Zone 1, 2, and 3. Zone 1 refers to the area below the water capillary fringe where LNAPL is a discontinuous nonwetting phase. Zone 2 refers to the area below the LNAPL capillary fringe where LNAPL is a continuous nonwetting phase. Zone 3 refers to the area above the LNAPL capillary fringe where LNAPL is a continuous intermediate wetting phase. Each zone has unique attributes controlling LNAPL mobility
- Solutions for LNAPL releases at GSIs need to address transport of LNAPL in all three zones
- Modeling fluid saturations versus height in a porous media using a force balance is more complex than two forces and requires further research

A common theme with current solutions for LNAPLs at GSIs is their failure with time. Failure is defined as the observation of LNAPL down-gradient of the solution. A better understanding of these failures is advanced through a volume balance on a representative elementary volume (REV) of porous media at a GSI. Key factors controlling releases to surface water include inflows, natural losses, enhanced losses, and recovery of LNAPL in the REV. Furthermore, the timing of failure is dependent on the capacity of the REV to store LNAPL prior to releases to surface water.

A novel solution demonstrated in this thesis was the use of capillary barriers to limit LNAPL lateral migration. Herein, capillary barriers are defined as vertical walls of fine-grained media that preclude lateral movement of LNAPL via a capillary pressure less than the displacement pressure in Zone 2 and an elevated water capillary fringe in Zone 3. A capillary barrier alone can delay releases; however, the barrier will fail when LNAPL storage capacities are exceeded. In contrast, the use of a recovery well to deplete accumulating LNAPL, in combination with a capillary barrier, provides a sustainable solution. During a laboratory experiment, 92% of the delivered LNAPL held behind the capillary barrier was recovered by aggressively pumping at low water stages.

A second strategy explored to control LNAPL releases at GSIs was organoclay barriers. Herein, organoclay barriers are defined as vertical walls of organoclay-sand mixtures. Organoclay is hydrophobic and retains LNAPL via sorption. Using a “simple” organoclay barrier, breakthrough to surface water was observed when only 11% of the organoclay was saturated with LNAPL. Early failure was attributed to preferential pathways and slow water drainage. Adding vertical baffles and vertical coarse-grained drains improved the efficacy of organoclay

barriers. Fractions of the clay contacted at breakthrough were 43% and 34%, respectively, for baffles and drains.

A concern that arose from the sand tank studies was the necessary water capillary rise in the capillary barrier to preclude LNAPL migration in Zone 3. This led to an attempt to develop a force-based model describing LNAPL (intermediate wetting phase) saturations in Zone 3. The model would be beneficial to determine the vertical rise of LNAPL at sites with non-tidal conditions. Key factors included in the model include spreading coefficients and gravity. The model developed (Model 1) was compared to three-phase data. It was found that Model 1 had poor correlation to the data and lacked some key factor affecting saturations. The model was altered by raising Model 1 to the power of λ and adding the residual saturation, resulting in Model 2. Model 2 was compared to two-phase data and the Brooks-Corey equation and showed promising similarities.

The work described in this thesis provides a basis for future work on remediation solutions and mathematical models for LNAPLs at GSIs. Work could include development of strategies to enhance natural losses of LNAPLs at GSIs and further refinements to Model 1 and Model 2 to better capture factors controlling fluid saturations in Zone 3.

ACKNOWLEDGEMENTS

I would like to make the following acknowledgements:

- First and foremost, Chevron for providing the funding for this research.
- Dr. Tom Sale for his guidance and support. Working with him and all the brilliant minds he comes into contact with has been very rewarding.
- Dr. Julio Zimbron for his guidance and assistance as well as serving on my committee.
- Dr. Michael Ronayne for being a member of my committee
- Dr. Art Corey for his assistance, advice, and scholarship.
- All of the people who have worked at the Center for Contaminant Hydrology have been great companions. I would especially like to thank Gary Dick, Anna Skinner, Calista Campbell, Adam Byrne, and Wes Tulli for their assistance in performing experiments.
- Lastly, I would like to thank my family and friends for their continued support throughout my master's program.

TABLE OF CONTENTS

ABSTRACT.....	ii
ACKNOWLEDGEMENTS.....	v
LIST OF TABLES.....	x
LIST OF FIGURES.....	xi
1. INTRODUCTION.....	1
1.1 Problem Statement.....	1
1.2 Hypotheses.....	3
1.3 Organization.....	4
2. OVERVIEW OF PROCESSES.....	5
2.1 Factors Governing the Behavior of LNAPLs.....	6
2.1.1 Relevant Physical Properties of Fluids.....	6
2.1.2 Physical Attributes of Commons GSIs.....	9
2.1.3 Zones of LNAPL Occurrence.....	10
2.1.4 Volume Balance.....	17
2.1.5 Force Balance.....	18
2.2 Experimental Techniques.....	19
2.2.1 Previous Work.....	19
2.2.2 Materials.....	20
2.2.3 Methods.....	23

3. LABORATORY SIMULATION OF LNAPL BEHAVIOR AT GROUNDWATER	
SURFACE WATER INTERFACES	31
3.1 Effects of Water Table Fluctuations.....	31
3.1.1 Objective.....	31
3.1.2 Background.....	32
3.1.3 Experimental Design	33
3.1.4 Results	34
3.2 Capillary Barrier.....	38
3.2.1 Objective.....	39
3.2.2 Background.....	40
3.2.3 Experimental Design	42
3.2.4 Results	43
3.3 Organoclay Barrier.....	47
3.3.1 Objective.....	47
3.3.2 Background.....	48
3.3.3 Experimental Design	49
3.3.4 Results	50
3.4 Conclusion.....	55
4. FORCE BALANCE APPROACH TO A SATURATION MODEL	57
4.1 Literature Review	57

4.1.1 Two-Phase Models	57
4.1.2 Three-Phase Model.....	59
4.1.3 Importance of Interfacial Tensions.....	60
4.1.4 Use of Spreading Coefficient	62
4.2 Force Balance Model	63
4.2.1 Scenario and Assumptions.....	63
4.2.2 Force Balance	64
4.2.3 Intermediate Wetting Phase Saturation	67
4.2.4 Wetting Phase Saturation.....	68
4.2.5 Nonwetting Phase Saturation.....	69
4.3 Comparison of Model and Data	70
4.4 Conclusion.....	75
5. CONCLUSION.....	76
5.1 Key Results	76
5.2 Future Research.....	78
6. REFERENCES	81
7. APPENDIX A.....	89
8. SUPPLEMENTAL MATERIAL.....	90
8.1 Capillary Barrier Video.....	90
8.2 Organoclay Barrier Video	91

8.3 Improved Organoclay Barrier Video.....	92
--------------------------------------------	----

LIST OF TABLES

Table 1. Properties of common contaminants.....	9
Table 2. Common types of groundwater surface water interfaces.....	10
Table 3. Zones of LNAPL occurrence.....	16
Table 4. Fluorescent dye properties.....	22
Table 5. Characteristics of barrier experiments.....	43
Table 6. Properties of media.....	64

LIST OF FIGURES

Figure 1. 1920s well field in the San Joaquin Valley, California (San Joaquin Valley Geology, 2011) and 2011 well field in Weld County, Colorado (Colorado State University Field Trip, 2011).	2
Figure 2. Sheen formation on surface water (courtesy of Pat Hughes).	3
Figure 3. LNAPL moving as an intermediate wetting fluid at the air-water interface in coarse sand (Photo courtesy of Dr. Julio Zimbron).	7
Figure 4. Depiction of Zone 1.....	12
Figure 5. Depiction of Zone 2.....	13
Figure 6. Depiction of Zone 3.....	14
Figure 7. Representative Elementary Volume	17
Figure 8. Sand tank set-up with an organoclay barrier.	20
Figure 9. Grain size distribution for PM-199 organoclay.....	21
Figure 10. Set-up for second barrier in second organoclay experiment; blue organoclay, light gray coarse sand, dark gray formation sand.....	25
Figure 11. Experimental set-up for flow visualization experiments.....	28
Figure 12. Illustration of steps employed to convert digital images to horizontally averaged estimates of LNAPL saturation.....	30

Figure 13. LNAPL distribution in non-tidal (left) and tidal (right) conditions at high tide (fluorescent green is LNAPL, dark green is water, no green is air).	35
Figure 14. Comparison of LNAPL (leading edge) horizontal transport in tidal and non-tidal conditions.....	35
Figure 15. LNAPL transport in the presence of tidal cycles.....	36
Figure 16. LNAPL thickness in well compared to thickness in formation.....	38
Figure 17. Relationship between LNAPL thickness and tidal level.	38
Figure 18. Capillary rise within a capillary barrier compared to the surrounding formation.	39
Figure 19. Capillary barrier experiment with two wells and a capillary barrier.....	42
Figure 20. LNAPL build-up due to capillary barrier and corresponding saturation curve obtained from transformation of the digital image to LNAPL saturation.	44
Figure 21. Graph of LNAPL (diesel) recovered in the capillary barrier with recovery experiment.	46
Figure 22. Depressed capillary rise in organoclay barrier compared to the formation.....	47
Figure 23. Second organoclay experiment with HDPE baffles and coarse-grained drains.	50
Figure 24. First organoclay barrier experiment showing overtopping and the corresponding saturation curve obtained from transformation of the digital image to LNAPL saturation.....	51

Figure 25. First organoclay barrier experiment at failure, showing preferential flow and the corresponding saturation curve obtained from transformation of the digital image to LNAPL saturation.....	52
Figure 26. First barrier in second organoclay experiment, with 3 HDPE baffles, at failure and the corresponding saturation curve obtained from transformation of the digital image to LNAPL saturation.....	53
Figure 27. Second barrier in second organoclay experiment, with drains, at failure and the corresponding saturation curve for second barrier obtained from transformation of the digital image to LNAPL saturation.....	54
Figure 28. Contact angle for a gas-liquid-solid system.	61
Figure 29. Sand grain in an REV and LNAPL wicking up a sand grain.	66
Figure 30. Data from Vizika and Lombard (1996) shown as dots compared to Model 1 shown as solid lines (green is air, red is LNAPL, and blue is water).....	71
Figure 31. Graph depicting fine sand data (Brooks and Corey, 1964) and models.....	73
Figure 32. Graph depicting volcanic sand data (Brooks and Corey, 1964) and models.....	73
Figure 33. Graph depicting glass beads data (Brooks and Corey, 1964) and models.	74

1. INTRODUCTION

1.1 Problem Statement

Anthropogenic use of petroleum liquids extends back thousands of years (The New Encyclopædia Britannica, 2005). Through time, use of petroleum liquids throughout the world has expanded to a current peak in excess of 87.4 million barrels a day (U.S. Energy Information Administration, 2011). Concurrently, best management practices for production, transmissions refining, and storage of petroleum have improved dramatically. Evolution of practices is exemplified by early oil and gas exploration involving frequent blow-outs, unlined earthen reservoirs, and wooden pipelines. In contrast, modern methods include directional drilling practices, blow prevention techniques, and dual storage tanks with leak detection at retail sites (Figure 1). These modern methods have dramatically reduced the frequency of petroleum releases to subsurface settings.



Figure 1. 1920s well field in the San Joaquin Valley, California (San Joaquin Valley Geology, 2011) and 2011 well field in Weld County, Colorado (Colorado State University Field Trip, 2011).

By the 1960s, the combination of expanding use of petroleum products and chronic releases associated with the era led to circumstances where rivers were catching on fire across North America (U.S. Environmental Protection Agency (U.S. EPA), 2012). Public outrage with burning rivers played a large role in the creation of the Clean Water Act (U.S. EPA, 2011). The Clean Water Act (CWA) created new regulations regarding point and nonpoint discharge of contaminants to surface water (U.S. EPA, 2011).

Today, releases of petroleum liquids (herein referred to as Light Non-Aqueous Phase Liquids, LNAPLs) to subsurface settings have been greatly reduced due to improved practices and evolving environmental ethics. Unfortunately, we are still living with the legacy of past practices and releases of LNAPL to surface water still occur. A common endpoint for releases to

surface water are visual sheens (Figure 2) leading to adverse publicity and violations of the CWA (U.S. EPA, 2011).



Figure 2. Sheen formation on surface water (courtesy of Pat Hughes).

Common solutions for LNAPL releases to surface water (sheens) include adsorbent booms, sheet-pile walls, and hydraulic recovery of LNAPL. Common limitations of these approaches include adverse impacts to riparian zones, limited effectiveness, high cost, and lack of sustainability.

1.2 Hypotheses

The overarching vision of this thesis is that an understanding of LNAPL behavior near groundwater-surface water interfaces (GSIs) will facilitate effective, sustainable, and lower cost solutions for LNAPL releases to surface water. Supporting hypotheses include:

- Tank studies using fluorescing dyes will facilitate novel insights regarding processes controlling LNAPLs at GSIs

- A LNAPL volume balance on a representative element of subsurface at a GSI can be used to identify hybrid remedies relying on passive barriers and enhanced natural losses
- Water table fluctuations will retard LNAPL migration
- Barriers with modified capillary properties can be employed to control the advancement of LNAPL as an intermediate wetting phase
- Synergies can exist between capillary barriers and LNAPL recovery
- A first principle force balance based on spreading coefficients, gravity, and soil properties can be used to develop a model to predict fluid saturations in two and three-phase systems

1.3 Organization

Chapter 2 presents an overview of processes governing LNAPL behavior. Two subsections in this chapter discuss factors that govern the behavior of LNAPLs and experimental techniques used to observe LNAPL behavior. Chapter 3 presents six laboratory experiments and associated results. The experiments focus on LNAPLs at GSIs in tidal versus non-tidal conditions, with capillary barriers present, and with organoclay barriers present. Chapter 4 presents a model for estimating fluid saturations versus elevation in two and three-phase systems. The model uses a force balance approach. Hysteresis and entrapment are not addressed. Lastly, Chapter 5 presents a summary of key results of this thesis and suggestions for future work.

2. OVERVIEW OF PROCESSES

World reliance on petroleum has grown to 87.4 million barrels a day. The U.S. alone consumes over 18 million barrels of petroleum products a day (U.S. Energy Information Administration, 2012). Uses for petroleum include fuels for transportation, fuel for heating, and feed stock for chemical processes. Petroleum released to the subsurface is referred to as a Light Non-Aqueous Phase Liquid (LNAPL). Common LNAPLs include diesel, gasoline, jet fuel, and lubricants (Dwarkanath et al., 2002; Charbeneau, 2000). Historical practices have led to the frequent occurrence of LNAPLs in the subsurface at almost all petroleum facilities. Primary concerns with LNAPLs in subsurface settings include impacts to groundwater and surface water quality. LNAPL impacts to surface water are a common issue due to the fact that petroleum facilities are often adjacent to surface water bodies including rivers, estuaries, harbors, and wetlands.

This chapter provides an overview of factors that govern the behavior of LNAPL near GSIs.

This includes:

- Relevant physical properties of LNAPLs
- Physical and hydrologic attributes of common GSIs
- A description of three common types of LNAPL occurrence in porous media
- A LNAPL-GSI conceptual model based on a LNAPL volume balance for a representative element of porous media at a GSI
- An exploratory attempt at using a force balance to estimate fluid saturations in unsaturated porous media

In addition, this chapter presents an overview of experimental techniques employed in subsequent sections.

2.1 Factors Governing the Behavior of LNAPLs

This subsection presents relevant physical properties of LNAPLs, physical and hydrologic attributes of common GSIs, a description of three common types of LNAPL occurrence in porous media, a LNAPL-GSI conceptual model based on a LNAPL volume balance for a representative element of porous media at a GSI, and an introduction to using a force balance to estimate fluid saturations in unsaturated porous media.

2.1.1 Relevant Physical Properties of Fluids

LNAPL impacted GSIs are multiple component systems including air, LNAPL, water, solid porous media, and microbial communities. The following introduces relevant physical properties of fluids that are employed in subsequent sections.

2.1.1.1 Wetting and Phase Continuity

A key concern with fluids in a porous media is the arrangements of fluids in pore space and the continuity of the phases. Herein:

- Air is treated as a nonwetting phase existing in the largest pores without direct contact with the porous media. Air can exist as either a continuous or discontinuous (residual) phase.
- Water is treated as the wetting phase forming a continuous phase about the porous media and filling the smallest pores. Herein, water is assumed to always be present as a continuous wetting phase.
- LNAPL may exist as an intermediate wetting phase or as a nonwetting phase. In porous media where air and water are present as continuous phases, LNAPL will act as an

intermediate wetting phase (Figure 3). This follows Charbeneau (2000), Wilson et al. (1990), and Keller et al. (1997). If air is not present as a continuous phase, LNAPL exists as a nonwetting phase which can exist as a continuous or discontinuous (residual) phase.

Critically, for a fluid to flow in a porous media, it must be present as a continuous phase.



Figure 3. LNAPL moving as an intermediate wetting fluid at the air-water interface in coarse sand (Photo courtesy of Dr. Julio Zimbron).

2.1.1.2 Interfacial Forces

Imbalanced forces exist across air-liquid, liquid-liquid, and liquid-solid interfaces (Corey, 1986). These forces are attributed to similarities and/or dissimilarities in the polarity of the phase. As an example, polar water molecules are typically most attracted to polar surfaces of natural porous media. Next, molecules in petroleum range from polar to nonpolar and are more attracted to water than porous media. Last, nonpolar gases (N_2 and O_2) are most attracted to petroleum liquids. Interfacial forces between phases lead to:

- LNAPL imbibing across air-water interfaces (i.e. sheen formation across surface water).

The propensity of a fluid to spread between two fluids (i.e. air and water) is characterized by the spreading coefficient:

$$S_c = \sigma_{aw} - (\sigma_{an} + \sigma_{ow}) \quad (1)$$

where σ are interfacial tensions [F/L or M/T²] and the subscripts a, n, and w represent air, LNAPL, and water phases, respectively (Padday 1992; Blunt et al., 1995; Keller et al., 1997; Vizika and Lombard, 1996). A positive spreading coefficient correlates to LNAPL spreading between water and air (Blunt et al., 1995; Keller et al., 1997; Vizika and Lombard, 1996)

- Air and LNAPL becoming entrapped in porous media as discontinuous phases when

$$P_c < P_d \quad (2)$$

where P_c is the capillary pressure [M/LT²] and P_d is the displacement pressure [M/LT²], where P_c is defined as:

$$P_c = P_n - P_w \quad (3)$$

where P_n is the LNAPL phase pressure [M/LT²] and P_w is the water phase pressure [M/LT²]. The displacement pressure is the pressure required to displace one fluid from a pore by another fluid (Corey, 1986). In the scenarios discussed in this thesis, the displacement pressure will refer to LNAPL displacing water from the pore

- The need for P_c in excess of P_d for a nonwetting fluid to invade a fully saturated media. If P_d is greater than P_c , LNAPL will not be able to displace water from the pores and will become immobile (Corey, 1986; Wilson et al., 1990; API, 2002)

All of the above principles are central to subsequent developments in this thesis. Other relevant fluid properties include specific gravity, absolute viscosity, aqueous solubility, vapor pressure, and propensity to degrade. Table 1 presents key properties for common contaminants.

Table 1. Properties of common contaminants.

Chemical	Specific Gravity	Absolute Viscosity (cP)	Interfacial Tension (with water; dyne/cm)	Surface Tension (dyne/cm)	Water Solubility (mg/L)	Vapor Pressure (mm Hg)	Propensity to Degrade**
Benzene	0.8737	0.6028	35	28.9	1.75E+03	9.52E+01	Aerobic / Anaerobic
Ethylbenzene	0.867	0.678	35.5	31.48	1.52E+02	7.00E+00	Aerobic / Anaerobic
Toluene	0.8623	0.552	36.1	30.9	5.35E+02	2.81E+01	Aerobic / Anaerobic
o-Xylene	0.8802	0.809	36.06	32.51	1.75E+02	6.60E+00	Aerobic / Anaerobic
Chlorobenzene	1.1063	0.799	37.4	35.97	4.66E+02	1.17E+01	Aerobic / Anaerobic
Trichloroethene (TCE)	1.4679	0.566	34.5	29.5	1.10E+03	5.79E+01	Anaerobic
Crude Oil	0.70-0.98	8-87	-	24-38	-	-	-
Diesel fuel	0.80-0.85	1.1-3.5	50	25	-	-	-
Gasoline	0.7321	0.45	50	21	-	-	-

*Data from Mercer and Cohen (1990) except where noted otherwise

** EPA, 1998

2.1.2 Physical Attributes of Commons GSIs

Groundwater surface water interfaces occur in a wide variety of hydrologic and geologic settings. A key concern with LNAPL as GSIs is the frequency and magnitude of water level fluctuations. A list of common GSIs and factors controlling water level fluctuations is given in Table 2. The significance of water level fluctuations is addressed in a subsequent section.

Table 2. Common types of groundwater surface water interfaces.

Setting		Reasons for Water Level Fluctuation	Examples	
Salt Water	Littoral	Coast (Beaches)	Storm surges, tides, tsunamis, hurricanes	Pacific U.S.
		Estuaries	Storm surges, tides, tsunamis, hurricanes	Hudson River, NY; Galveston Bay, TX, Hong Kong, China
		Harbors	Storm surges, tides, tsunamis, hurricanes	San Diego, CA; Norfolk, VA; Yokosuka, Japan; Sydney, Australia
Fresh Water	Fluvial	Deltas	Storm surges, tides, tsunamis, hurricanes, flow variations from inflow	Mississippi near New Orleans, LA; Ganges, India; Danube, Europe
		Large Rivers	Seasonal flow variations from inflow	Mississippi, U.S.; Yangtze, China; Nile, Africa
		Small Rivers	Precipitation events	Cache La Poudre, CO; Clark Fork, MT
	Lake	Large	Weather patterns, flow variations from inflow	The Great Lakes, U.S.; Victoria, Africa; Manitoba, Canada
		Small	Flow variations from inflow	Lake Harriet, MN; Lake Loveland, CO
	Wetlands		Weather patterns, flow variations from inflow	Amazon river basin, Brazil; Pantanal, Brazil; West Siberian Plain, Russia
	Springs and Seeps		Seasonal precipitation events	-

2.1.3 Zones of LNAPL Occurrence

LNAPLs occur in three distinct zones in porous media. Typically, it is thought that when an LNAPL is spilled it will travel downward until it reaches the top of the water table. Next,

LNAPL will migrate in the direction of the hydraulic gradient (towards a GSI). How the LNAPL migrates and the “rules” governing the transport of LNAPL to surface water are distinctly different depending on the presence and arrangement of air, LNAPL, and water in porous media. Building on this, three distinct zones of LNAPL occurrence have been identified. The fraction of the total LNAPL in each zone changes with water table fluctuations. The following reviews key attributes of the three primary zones of LNAPL occurrence. A summary of the key points is presented in Table 3, presented at the end of Section 2.1.3.4.

2.1.3.1 Zone 1

Zone 1 is the bottom zone in the subsurface where LNAPL is present and Zone 1’s upper limit is where LNAPL becomes a continuous phase. Zone 1 is where water is a continuous wetting phase and LNAPL is a discontinuous nonwetting phase. Minor discontinuous ganglia and blobs of air are common in Zone 1 due to biological degradation of dissolved phase LNAPL constituents and/or air entrapment by water table fluctuations. Migration of water is governed by Darcy’s Law. The LNAPL is immobile due to its presence as a discontinuous phase. The general condition for discontinuous LNAPL is $P_c < P_d$. This concept is central to understanding LNAPL recoverability as a function of water level. An illustrative photograph of Zone 1 is presented in Figure 4. Typically, the amount of LNAPL present in Zone 1 is at a maximum at high water levels and at a minimum at low water levels.

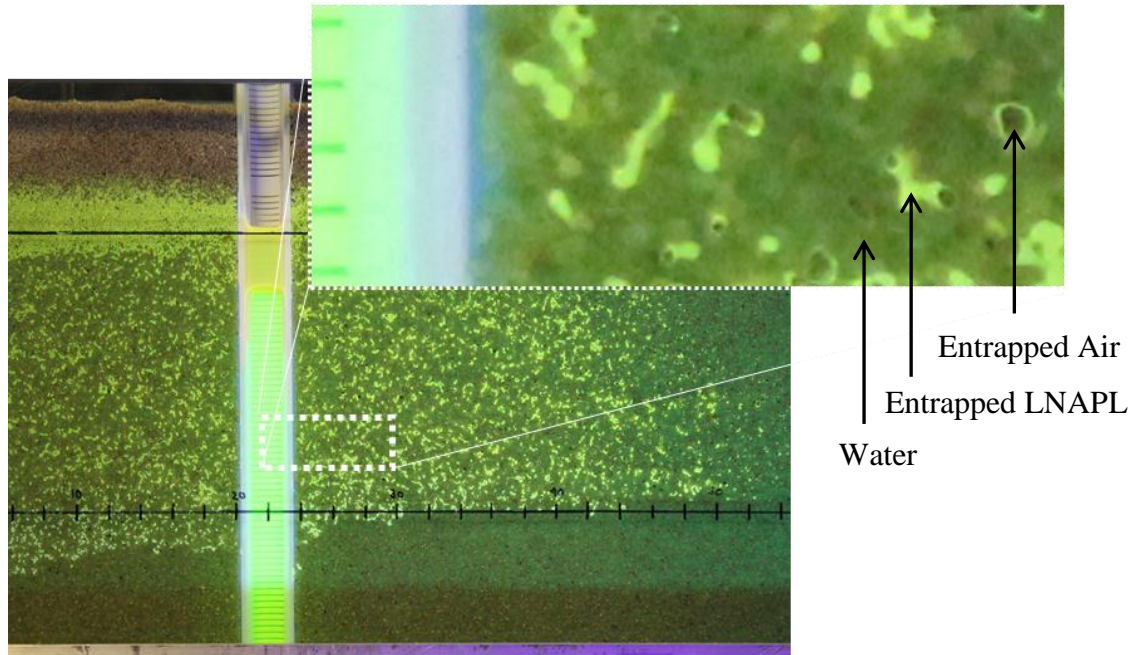


Figure 4. Depiction of Zone 1.

2.1.3.2 Zone 2

Zone 2 occurs above Zone 1 and Zone 2's upper limit is where air becomes a continuous phase. Zone 2 is where water is a continuous wetting phase and LNAPL is a continuous nonwetting phase. Again, minor discontinuous ganglia and blobs of air are common in Zone 2 due to biological degradation of dissolved phase LNAPL constituents and/or air entrapment by water table fluctuations. Migration of water and LNAPL is governed by Darcy's Law, wherein permeability is constrained by fluid saturations and flow is driven by gradients in fluid pressure. The necessary condition for LNAPL to invade porous media without LNAPL is $P_c > P_d$. This concept is central to employing capillary barriers to preclude LNAPL migration in Zone 2. An illustrative photograph of Zone 2 is presented in Figure 5. Generally, the fraction of the total LNAPL in a porous media in Zone 2 is at a maximum at low water levels and at a minimum at high water levels.

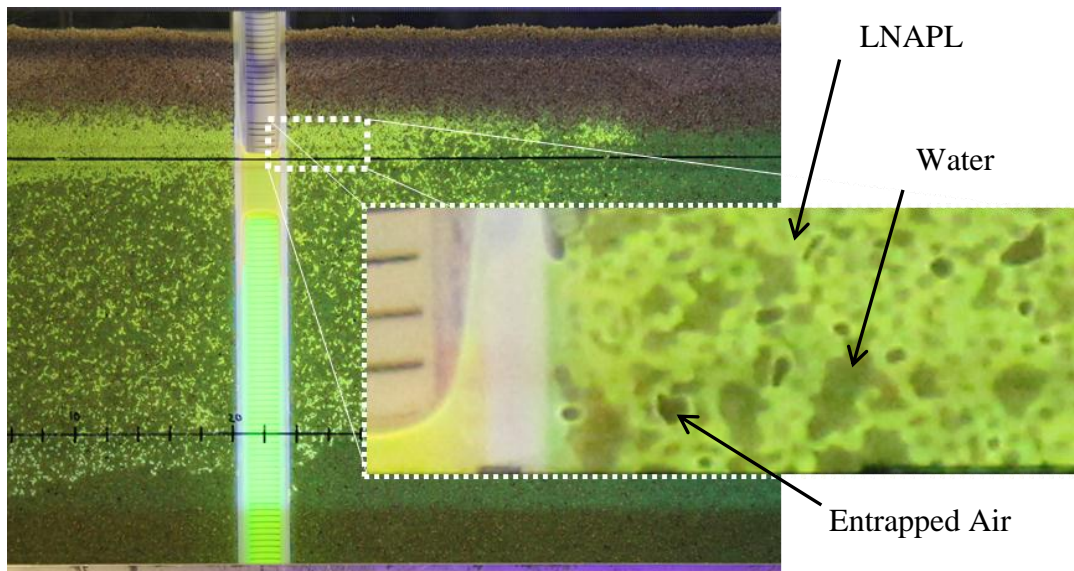


Figure 5. Depiction of Zone 2.

2.1.3.3 Zone 3

Zone 3 occurs above Zone 2 and Zone 3's upper limit is where LNAPL ceases to be found (unless a vadose zone is considered, Section 2.1.3.4). Zone 3 is where water is a continuous wetting phase, air is a continuous nonwetting phase, and LNAPL is a continuous intermediate wetting phase. This zone has received the least attention in literature and is the primary focus of this thesis. Migration of all three phases is governed by Darcy's Law. An interesting aspect of this zone is that initial LNAPL invasion into non-impacted media is governed by interfacial forces leading to LNAPL spreading along the air-water interface. Per laboratory studies, initial movement of LNAPL occurs into unimpacted media as an intermediate-wetting phase drawn by spontaneous imbibition. Spontaneous imbibition is due to capillary forces drawing the intermediate wetting fluid into the porous medium (Morrow and Mason, 2001). The LNAPL first moves through the media as a thin film or sheen. The LNAPL builds-up behind the film on top of the capillary fringe and then leaps forward. An illustrative photograph of Zone 3 is presented in Figure 6. The amount of LNAPL present in Zone 3 is less dependent on the water

level and more dependent on the LNAPL pool size and delayed drainage of LNAPL. There are two key differences between Zone 1 and Zone 3. First, Zone 1 LNAPL is immobile and Zone 3 LNAPL is mobile, and secondly, residual saturations are typically much smaller in Zone 3 than in Zone 1. The volume of residual LNAPL is central to understanding the ability for future contamination by dissolution and vaporization. Another interesting aspect of Zone 3 is that the presence of a continuous gas phase can enhance rates of biodegradation via release of reaction byproducts (CO_2 and CH_4) and entry of atmospheric oxygen. Zone 3 is the primary focus of the final chapter of this thesis exploring first principles analysis of fluid saturations.

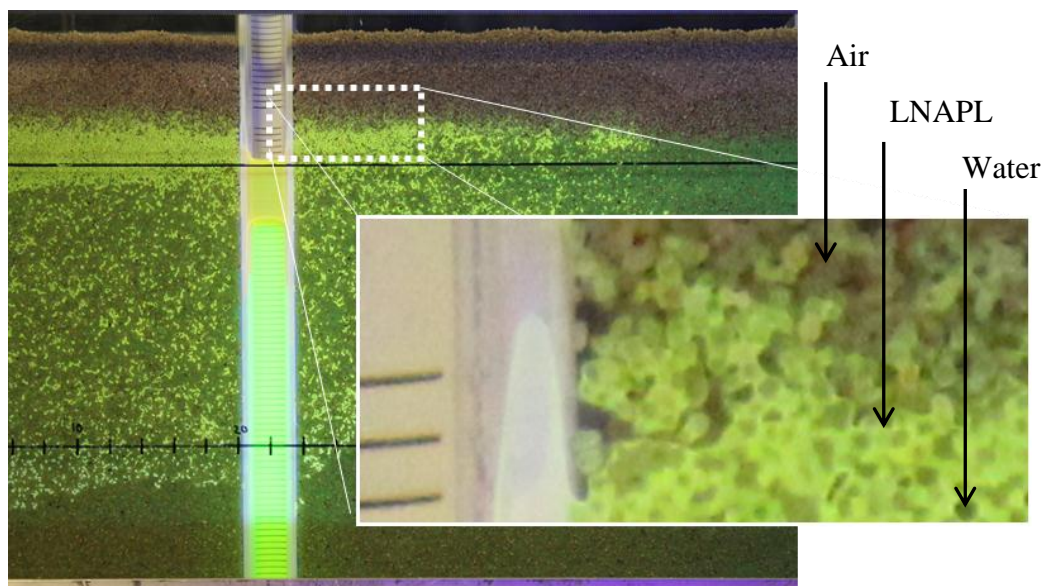


Figure 6. Depiction of Zone 3.

2.1.3.4 Vadose Zone

An argument can be made for a fourth zone, in the vadose zone above Zone 3. The vadose zone is similar to Zone 3 in that all three phases are continuous. The vadose zone differs from Zone 3 because the LNAPL is at a lower saturation and immobile horizontally. Vertical LNAPL migration occurs as a result of delayed drainage. Typically, the vadose zone is thickest in size at

low tide, however, the actual thickness depends on the range of the water table fluctuations. In addition, like Zone 3, air is present at large saturations which increases the amount of biodegradation and volatilization that occurs. The amount of LNAPL present in the vadose zone is different for imbibition and drainage cycles, however, overall, there is a minimal volume present so this zone is often disregarded.

Table 3. Zones of LNAPL occurrence.

Zones	Characteristics	Saturations*			Controls on LNAPL Saturation	Controls on LNAPL Stability	Formula regarding LNAPL Flux (Horizontal Flow) **
		S_a	S_n	S_w			
1	Water continuous phase, LNAPL discontinuous phase	0 to S_{ra}	$S_n \leq S_{rn}$	$S_w = 1 - S_n$	$P_c \leq P_d$, aqueous loss processes	Flux = 0 due to discontinuous LNAPL phase	$q_n = 0$
2	Water and LNAPL present as continuous phases	0 to S_{ra}	$S_n > S_{rn}$	$S_w = 1 - S_n$	$P_c > P_d$, LNAPL pool thickness, aqueous loss processes, hysteresis	LNAPL saturation, LNAPL properties, LNAPL gradient (elevation, slope, concentration)	$q_n = -\frac{k * k_r}{\mu_n} * \frac{dP}{dx}$
3	Water (wetting), LNAPL (intermediate wetting) and air (nonwetting) all present as continuous phases	$S_a > S_{ra}$	$S_n = 1 - S_w - S_a$	$S_w = 1 - S_n - S_a$	Delayed drainage, aqueous and vapor loss processes	LNAPL saturation, LNAPL properties, horizontal gradient of LNAPL pressure	$q_n = -\frac{k * k_r}{\mu_n} * \frac{dP}{dx}$

* S is the saturation and a, n, and w represent air, napl, and water phases. S_r is the residual saturation in the two-phase zones

** q_n is the LNAPL flux, k is the intrinsic permeability, k_r is the relative permeability, μ_n is the LNAPL viscosity, and P is the pressure

2.1.4 Volume Balance

The conceptual model presented in this section forms a basis for evaluating remedies for LNAPLs at GSIs, including limitations of current approaches and opportunities for more effective, sustainable, and/or lower cost solutions. The model begins with a representative elementary volume (REV) of porous media at a GSI and common LNAPL inflows and outflows (Figure 7). When this REV is in close proximity to a shoreline, it is referred to as a near-shore reference volume.

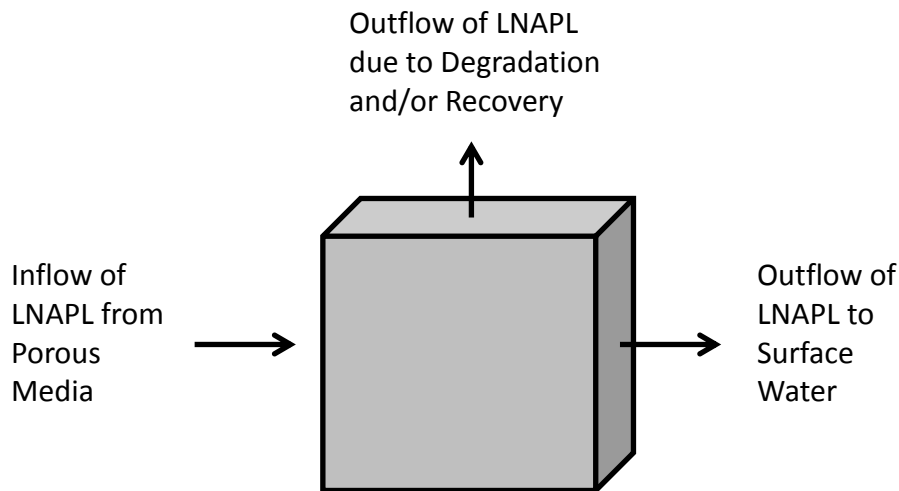


Figure 7. Representative Elementary Volume

Mathematically, Figure 7 leads to:

$$LNAPL_{in} - LNAPL_{sw} - LNAPL_D - LNAPL_R = \frac{dLNAPL}{dt} \quad (4)$$

where:

$LNAPL_{in}$ = inflow of LNAPL from up-gradient [L^3/T]

$LNAPL_{sw}$ = outflow of LNAPL to surface water [L^3/T]

$LNAPL_D$ = outflow of LNAPL due to natural and/or enhanced losses [L^3/T]

$LNAPL_R$ = outflow of LNAPL due to recovery [L^3/T]

$LNAPL$ = LNAPL volume in the REV [L^3]

t = time [T]

Discharge to surface water from the REV is conditional upon LNAPL being present in excess of the LNAPL storage capacity of the REV. Mathematically this is stated as:

$$LNAPL_{SW} > 0 \quad \text{when} \quad LNAPL > REV_{cap} \quad (5)$$

where REV_{cap} [L^3] is the LNAPL storage capacity of the REV. This conceptual model leads to a series of insights regarding remedies:

- Any remedy will fail at large time given insufficient losses ($LNAPL_D$) and recovery ($LNAPL_R$). Failure is defined as the observation of LNAPL down-gradient of the remedy
- Releases to surface water are dependent on all of the factors introduced in Equations (4) and (5)
- Remedy elements can include reduced inflow ($LNAPL_{in}$), increased storage capacity (REV_{cap}), increased losses ($LNAPL_D$), and/or increased recovery ($LNAPL_R$)

These points will be used in subsequent sections to address current remedies and opportunities for innovative solutions.

2.1.5 Force Balance

Current models for fluid saturations in porous media rely on fitting empirical models to data (Brooks and Corey, 1964; van Genuchten, 1980). Interestingly, these models do not rely on first

principle analyses of forces and, in particular, on how spreading coefficients control fluid saturations. An initial investigation into this topic is presented in Chapter 4.

2.2 Experimental Techniques

The following introduces experimental techniques that are common to sand tank studies presented in chapter 3. Presentation herein supports more rigorous discussions in subsequent sections. Content includes a review of previous work, materials, and methods.

2.2.1 Previous Work

To clearly understand LNAPL migration, one must focus on the pore level processes. To understand pore-scale processes, experiments have been performed using: 1) two dimensional sketched glass plates (Wilson et al., 1990); 2) etched silicon wafers (Keller et al., 1997); and 3) trace paper to draw plume movement in sand tank studies (Schwille, 1988; Schroth et al., 1995). Wilson et al. (1990) chose to use etched glass micromodels to see how fluids displace each other within individual pores. Wilson et al. (1990) realized the importance of understanding how fluids become entrapped within the pores to determine the fluids ability to migrate. To enhance visualization of contaminated versus uncontaminated media, dyes have been used. The experiments performed by Wilson et al. (1990) used a red dye (Soltrol) for the contaminant but it did not fluoresce. Schwille (1998) used fluorescein to dye contaminants dissolved in water and oil red for the non-aqueous phase liquid, therefore, only the aqueous phase fluoresced. Neither Wilson et al. (1990) or Schwille (1998) used black lights to enhance the visualization of the LNAPL or water. Research regarding the use of fluorescent dyes will be discussed in a subsequent section.

2.2.2 Materials

The following describes materials used in experiments associated with this thesis.

2.2.2.1 Sand Tank Set-up

A two-dimensional sand tank was utilized for the experiments. The internal dimensions of the tank were 180 cm (horizontal length in the direction of flow) by 38.5 cm (vertical height) by 5.3 cm (depth). The front and back face were glass and the bottom and ends were aluminum. The top of the tank was open to the atmosphere. The right end of the tank had a permeable screen to allow flow of water but prevented sand grains from entering into the Fluorinated Ethylene Propylene (FEP) 1/8" tubing (United States Plastic Corp, Lima, OH) used for altering water table levels (discussed subsequently). The screen was constructed from Round Hole Perforated stainless steel sheets (McMaster-Carr, Atlanta, GA) bent to 2.5 cm wide by 38.5 cm long by 5.3 cm deep. The sheet was covered in type 304 stainless steel 50x50 wire mesh (McMaster-Carr, Atlanta, GA). Figure 8 shows a picture of the sand tank.

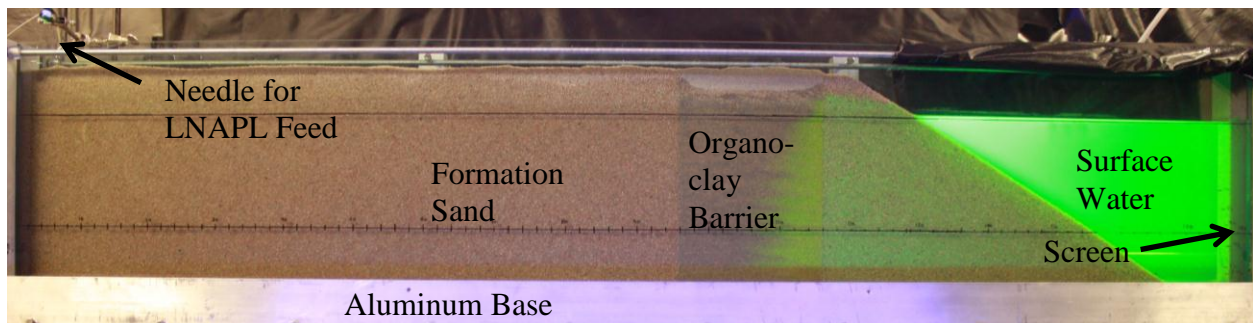


Figure 8. Sand tank set-up with an organoclay barrier.

2.2.2.2 Porous Media

Four sands acquired from Colorado Silica Sand (Colorado Springs, CO) were used in the experiments.

- Medium (10-20) sand was used for the formation
- Fine (100) sand was used for the capillary barriers
- Mid-sized (20-40) sand was used to mix with the organoclay (see below)
- Coarse (8-12) sand was used as a high conductivity drainage layer in one of the organoclay barrier experiments

All sand was washed prior to use to reduce fines in the sand.

A mix of organoclay and sand in a 1:3 ratio was used for the organoclay barriers. The organoclay used in the experiments was PM-199 from CETCO (Hoffman Estates, Illinois). The grain size distribution of PM-199 was determined (Figure 9) to ensure the sand used (20-40 Colorado Silica Sand) was of the same size as the PM-199 organoclay. Sand was used in the mixture instead of clay to allow for adequate conductivity of the water through the barrier. Herein, organoclay refers to the mixture of organoclay-sand used in the barriers.

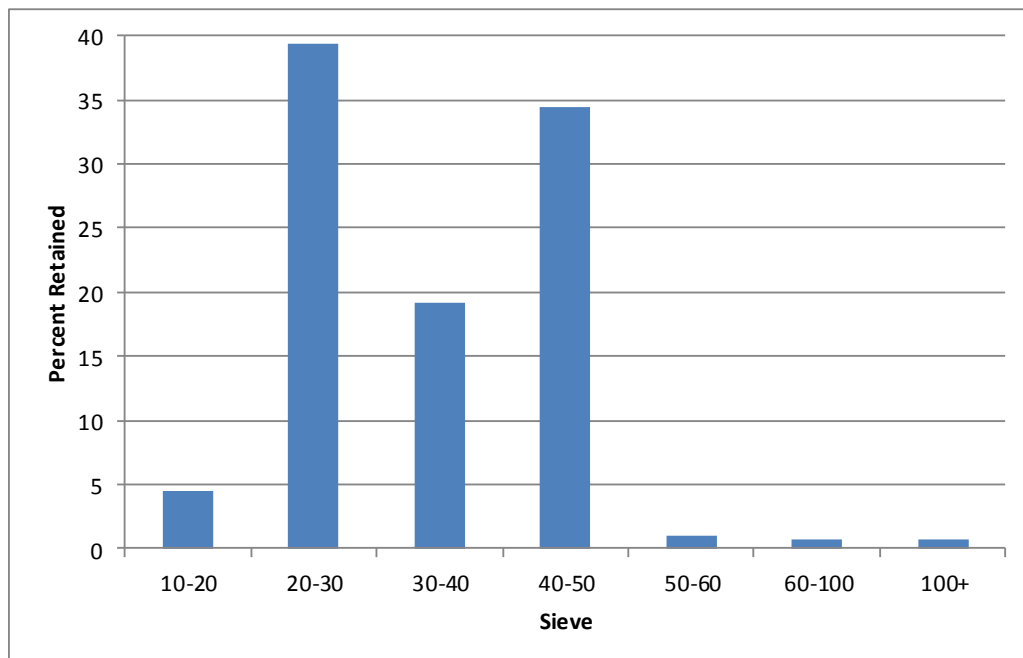


Figure 9. Grain size distribution for PM-199 organoclay.

2.2.2.3 Liquids and Dyes

Fluorescent dyes and UV lights (black lights) were employed to enhance visualization of LNAPL behavior in the sand tanks. Research at Colorado State University by Ryan Taylor and Lee Ann Doner used fluorescent dyes and black lights for this purpose. Ryan Taylor, as presented in Sale et al., 2007, used a fluorescent dye (BSL 715, a.k.a. StayBrite) in tracer tests to determine LNAPL flow rates through wells and the adjacent formations. Lee Ann Doner, as presented in Chapman et al., 2012, performed research looking at diffusion of contaminant into and out of low permeability zones. Water containing Fluorescein was used to visually observe contaminant storage and release in low permeability zones. The use of fluorescent dyes in the above studies was the basis for their use in the experiments in this thesis. Common fluorescent dyes and their properties are shown in Table 4. The key characteristic of LNAPL fluorescent dyes is that they must be insoluble in water (hydrophobic).

Table 4. Fluorescent dye properties.

Dye	Color	Fluoresce		Gs	Solubility in Water	Ref.	
		Color	Peaks				
Fluorescein	Orange to Red	Green	540		Soluble	a	
Diesel	Amber	Blue	490		0.83	Insoluble	b
BSL 715 StayBrite	Dark Red	Green	550	585	0.89	Insoluble	c
OIL-GLO 22	Dark Red	Yellow	580	565	0.89	Insoluble	d
OIL-GLO 33	Amber	Green	495		0.98	Insoluble	d
OIL-GLO 40	Amber	Blue	490		0.93	Insoluble	d
OIL-GLO 44	Dark Red	Yellow / Green	540	590	0.93	Insoluble	d
OIL-GLO 50	Red	Red	600		0.85	Insoluble	d

a ScienceLab.Com

b Experimentally determined

c Bright Solutions

d Spectronics Corporation

For all the experiments, diesel was used as the LNAPL. The diesel was obtained from a gas station located in Fort Collins, CO. Diesel has low solubility in water, low volatility, and a positive spreading coefficient. The diesel was dyed with StayBrite (Brite Solutions Inc., Hollywood, FL). StayBrite was added to the diesel at a concentration of 0.1% on a weight basis.

All experiments were conducted using Fort Collins tap water. Water for the experiment was degassed by holding it at -24 in Hg for 3 hours. The water was dyed with Fluorescein (Science Lab, Houston, TX). Fluorescein was added to the water at a concentration of 0.25% on a weight basis.

2.2.3 Methods

The following describes methods employed in the experiments presented in this thesis.

2.2.3.1 Materials Placement

The left hand and center portions of the tank were filled with sand to a height of 36 cm. On the right hand side, the sand tapers from 36 cm to 0 cm. Water was fed into the tank at 25 mL/min. to a height of 36.5 cm, to fully saturate the sand. The sand tank was allowed to stand overnight prior to lowering the water level to 28 cm, corresponding to high stage. Select experiments contained wells, capillary barriers, and organoclay barriers.

Wells were constructed so they were against the front face of the tank for observation. The wells were made from a 2.54 cm diameter PVC well screen, with two sections of 0.5 mm slots (Johnson Screens, Houston, TX). The PVC was cut in half length-wise to allow for visualization into the well. The wells were 38 cm long. To prevent sand grains from entering the well, Tygon vinyl tubing (McMaster-Carr, Atlanta, GA) was sliced length-wise and slid on to the well edges.

Wells were pressed against the face of the tank utilizing 0.5 in diameter PVC pipe cut to act as a wedge.

Vertical walls of fine-grained sand, referred to as capillary barriers, were constructed so they were 4 cm wide by 36 cm high by 5.3 cm deep. To build a barrier, two sheets of high-density polyethylene (HDPE; Fort Collins Plastics, Fort Collins, CO), 2 mm thick, were cut to 36 cm by 5.3 cm. The two pieces of HDPE were connected by three pieces of All Thread (Ace Hardware) and nuts (Ace Hardware) to keep the HDPE pieces 4 cm apart. This form was then inserted into the tank at the desired position and filled with fine Colorado Silica Sand to create the capillary barrier. As the form was filled with fine sand, the rest of the formation was filled with medium (10-20) Colorado Silica Sand. Once the tank was filled with all required sand, the form was removed.

Three different types of organoclay barriers were used. The first type was simply a 20 cm wide vertical organoclay barrier. The construction of this organoclay barrier was the same as for the capillary barrier. The second type of organoclay barrier was 15 cm in width and constructed as previously mentioned. After removal of the form, three 4 cm by 5.3 cm HDPE pieces, 2 mm thick, (Fort Collins Plastics, Fort Collins, CO) were emplaced in the top of the barrier, perpendicular to flow. The HDPE pieces acted as baffles and were equally spaced within the barrier. The third type of organoclay barrier had vertical coarse sand layers between the organoclay layers (Figure 10). Overall, the barrier was 20 cm thick and had 4 organoclay layers and 3 coarse sand layers. The layers were constructed by using multiple HDPE pieces connected by All Thread and nuts to keep proper spacing between the HDPE pieces. The construction was then similar to the capillary barriers.

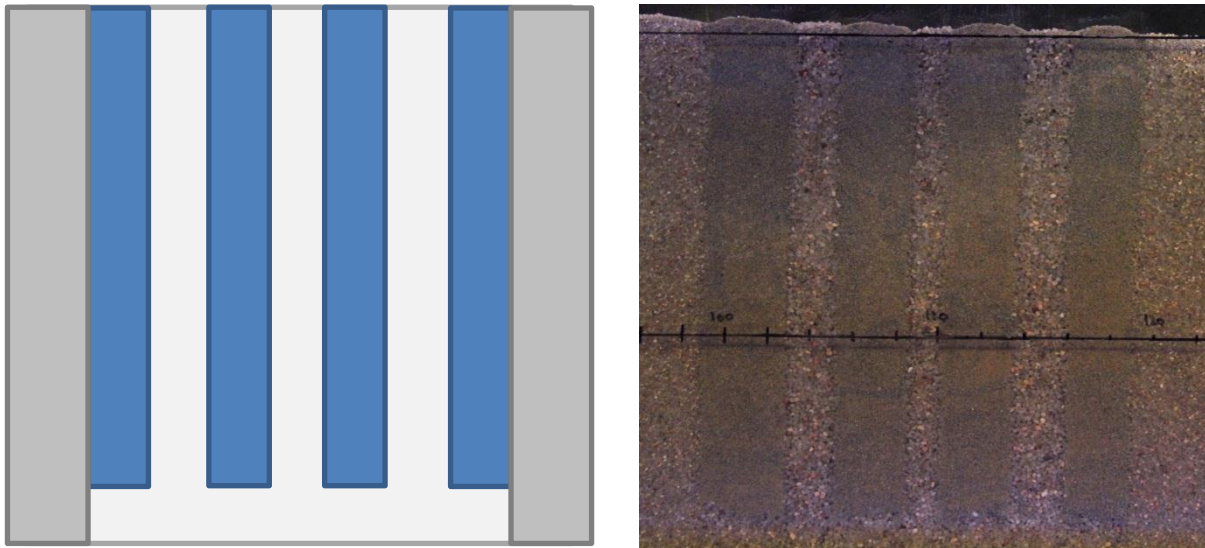


Figure 10. Set-up for second barrier in second organoclay experiment; blue organoclay, light gray coarse sand, dark gray formation sand.

2.2.3.2 Fluid Levels

The LNAPL was introduced to the left hand side of the tank 1 cm above the top of the sand. A compact multichannel peristaltic pump (REGLO model, ISMATEC, Glattbrugg, Switzerland), pumping at a rate of 6 mL/hr, was used to introduce the LNAPL to the tank. An 18G 1 ½ syringe needle (VWR, Radnor, PA) was at the end of the FEP tubing and allowed for LNAPL to enter the tank at a precise location.

Water levels were controlled by a compact multichannel peristaltic pump. The pump was connected to a Microsoft Windows computer that controlled operation of the water table. Water table fluctuations (tidal cycles, 6 hour rise and 6 hour fall) were automated using a Microsoft Windows computer equipped with LabView 8, a National Instruments (Austin, TX) computer program. Water was held in a storage tank when not in use and was pumped into the right hand side of the tank, inside the permeable screen. The FEP tubing was set at a fixed height to ensure

low water levels were the same for each cycle. Water was pumped at a rate so the water reached high/low at the six hour mark and did not sit at high or low levels for extended periods of time.

2.2.3.3 Porous Media and Fluid Properties

Select properties of the porous media and fluids were determined experimentally. The methods for determining porosity, density, and interfacial tensions are discussed in this section.

2.2.3.3.1 Porosity

Porosity was determined using the following relationship:

$$\phi = 1 - \frac{\rho_b}{\rho_s} \quad (6)$$

where ϕ is the porosity [dimensionless], ρ_b is the bulk density [M/L³], and ρ_s is the particle density [M/L³]. Particle density was assumed to be 2.65 gm/cm³. The bulk density was calculated by:

$$\rho_b = \frac{m_s}{v_s} \quad (7)$$

where m_s is the mass of the sand [M] and v_s is the volume of the sand [L³]. The mass of a known volume of sand was measured in the laboratory.

2.2.3.3.2 Fluid Density

Density of the fluids was determined by measuring the weight of the fluid in a fixed volume.

$$\rho_f = \frac{m_f}{v_f} \quad (8)$$

where ρ_f is the density of the fluid [M/L³], m_f is the mass of the fluid [M], and v_f is the volume of the fluid [L³].

2.2.3.3.3 Interfacial Tensions

Interfacial tensions were determined between water-air, LNAPL-air, and LNAPL-water. A DuNouy tensiometer (70545 model, CSC Scientific Company, Fairfax, VA) was used for each measurement and followed standard test method outlined in ASTM D971 (ASTM, 2012).

2.2.3.4 *Digital Photographs*

2.2.3.4.1 Lighting

Two 40W, T12 black lights (Ace Hardware, Fort Collins, Co) were employed to excite fluorescence. The black lights were 120 cm long and were centered in front of the tank. One black light was mounted 5 cm below the tank facing upwards and the other was 25 cm above the tank facing downwards. Both lights were 40 cm away from the tank, horizontally.

White lights were employed as a complement to the UV light. White light provided the ability to see non-fluoresced elements of the experiment. In addition, white lights provided enough ambient light in the room for the cameras to focus. The source of white light consisted of two 10W compact fluorescent single-bulb stand mounted portable lights (Ace Hardware, Fort Collins, CO) set-up 100 cm diagonally out from the front corners of the tank. The lights were raised so the light was 10 cm from the ceiling (indirect lighting) to prevent reflection in the glass.

2.2.3.4.2 Cameras

Tripods and cameras were set-up and automated to take pictures of the experiment at intervals of 7.5 or 15 minutes. One Canon Rebel T2I camera (Canon, Melville, NY) was placed 150 cm away, centered on the entire tank. A second Canon Rebel XSI camera (Canon, Melville, NY) was placed 120 cm away from the tank, centered vertically on the tank, and took pictures zoomed in on a 45 cm wide portion of the tank. As the LNAPL transported along the air-water

interface, this second camera was moved manually to capture the leading edge of the spill. Each camera was controlled by a Microsoft Windows computer using EOS Utility software (Canon, Melville, NY). Pictures were taken every 15 minutes for the zoomed out camera and every 7.5 minutes for the close up pictures. Figure 11 shows the room set-up for the experiments.

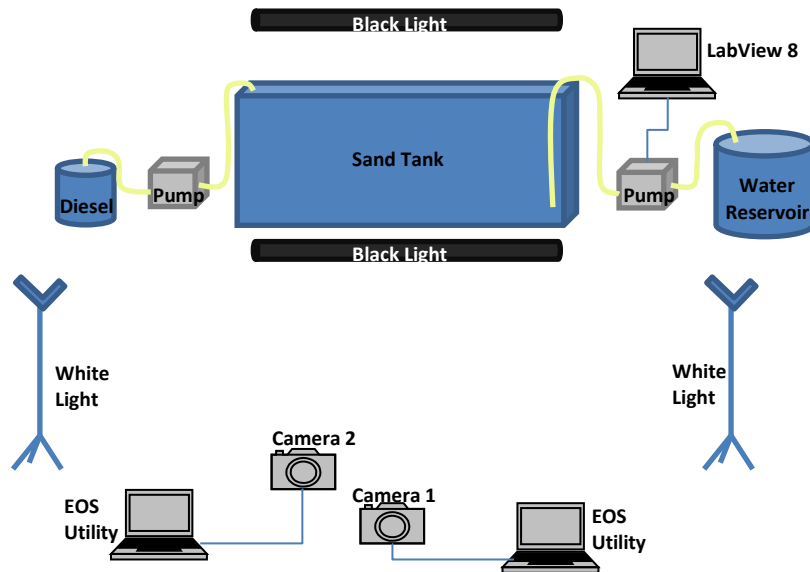


Figure 11. Experimental set-up for flow visualization experiments.

2.2.3.5 Data Compilation

The fluorescent dyes used in the experiments enhanced the visualization of the LNAPL's migration. In addition, technological advances with digital cameras and image analyzing software increased the ability to look at and analyze the media at the pore scale. In more detail, utilizing Adobe® Photoshop® 7.0 (Adobe®, San Jose, CA) and MATLAB® (MathWorks® Natick, MA), photos taken during experiments were digitally enhanced to create binary pictures and LNAPL saturation curves. Dr. Julio Zimbron is credited with the initial process of creating saturation curves from digital images. To create a saturation curve, the first step is to adjust the color balance in Adobe® Photoshop® 7.0 allowing the enhancement of LNAPL, while

darkening the remaining portions of the photograph. The next step was to generate a simple program in MATLAB® to create a binary photo (see Appendix A). The fluorescing LNAPL was transformed to white and all other portions of the photo were converted to black. To do this, a luminescence level was chosen to accurately match the black and white photo to the original. The MATLAB® program then averaged every two rows of pixels to measure the saturation and created a saturation curve. Figure 12 shows the transformation of a photo and the LNAPL saturations up and down gradient of a capillary barrier. The first saturation curve, representing the media to the left of the capillary barrier, illustrates how well MATLAB® creates saturation curves. Near the top portion of the curve, the saturation is shown as approximately 0.95 which is discernible in the three photos. The saturation curves allowed for easy comparison of saturations at failure for the barriers. Videos of the experiments were made with Windows Live™ Movie Maker (Microsoft Corporation, Redmond, WA) and Adobe® Premier® Elements 9 (Adobe®, San Jose, CA).

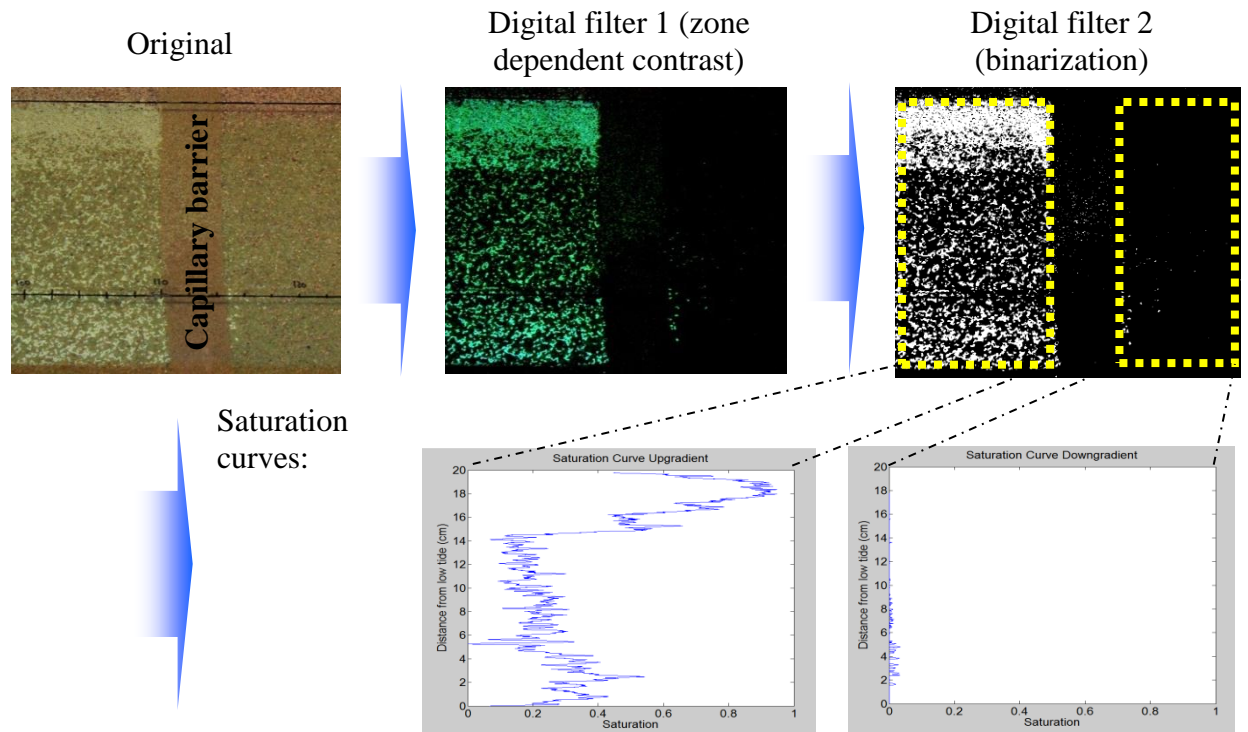


Figure 12. Illustration of steps employed to convert digital images to horizontally averaged estimates of LNAPL saturation.

3. LABORATORY SIMULATION OF LNAPL BEHAVIOR AT GROUNDWATER SURFACE WATER INTERFACES

Six experiments are presented in this chapter. The experiments provide insight regarding LNAPL behavior in porous media at GSIs. The first subsection looks at the effects of water table fluctuations on the migration of LNAPL. Two experiments are presented, one with a static water table and another with two water level cycles per day. The second subsection of this chapter explores capillary barriers as an option to limit LNAPL migration. Two capillary barrier experiments are presented, one looked at the efficacy of a capillary barrier and another evaluated the complementary benefits of recovering LNAPL up-gradient of the capillary barrier. The third section investigates the use of organoclay barriers as a means of retarding LNAPL migration. Two organoclay barrier experiments are presented, one that used a simple organoclay barrier and a second that included improvements to the barrier to increase sorption. Each section is broken down into four parts that address objectives, background information, experimental details, and results.

3.1 Effects of Water Table Fluctuations

3.1.1 Objective

The objectives of the water table fluctuation experiments presented in this section were to determine:

- The effect water table fluctuations have on LNAPL distribution
- The relationship between LNAPL thickness in wells versus the formation as a function of water levels

Throughout this thesis the phrase tidal cycles is used as a general term to describe cyclic water table fluctuations.

3.1.2 Background

Groundwater surface water interfaces are affected by hydrologic cycles that can be random or periodic (Table 2, presented in Section 2.1.2). With water table fluctuations, the fraction of LNAPL in Zone 1, 2, and 3 shifts. At high water levels, the majority of the LNAPL in the formation resides in Zone 1, with a minimum in Zones 2 and 3. As the water levels fall, residual LNAPL in Zone 1 is released and becomes part of Zones 2 and 3. At low stages, the quantity of mobile LNAPL in wells (and Zone 2) typically is at a maximum.

Historically, LNAPL thicknesses in wells have been used as an indicator of the amount of LNAPL in the formation and the need for remedial measures (Interstate Technology & Regulatory Council, 2009). Unfortunately, LNAPL in a well is only an indicator of LNAPL in Zone 2 (assuming vertical equilibrium). Zone 3 LNAPL is present under negative pressure, and correspondingly, does not move into the wells. Zone 1 LNAPL is present as a discontinuous phase and, therefore, is immobile and unable to enter wells. Furthermore, Zone 1 LNAPL is present at a pressure less than the adjacent water by P_d . Mathematically this is represented by:

$$P_N = P_W - P_d \quad (9)$$

where P_N is the capillary pressure of the LNAPL [M/LT^2] and P_W is the capillary pressure of the water [M/LT^2].

Given vertical equilibrium, the LNAPL thickness in the well can be related to capillary pressures (Charbeneau, 2000; API, 2002). The associated capillary pressures can then be related to

thicknesses of LNAPL in Zone 2. Farr et al. (1990) created a mathematical model that calculates the volume of mobile LNAPL as a function of the thickness of LNAPL in the adjacent well. The volume of LNAPL calculated in these equations corresponds to LNAPL in Zone 2. The equations only work in homogeneous materials, at vertical equilibrium, and does not account for residual or entrapped LNAPL. Kemblowski and Chiang (1990) and Pantazidou and Sitar (1993) developed equations that relate well thickness to formation thickness. The details of these equations are beyond the scope of this thesis. Farr et al. (1990) support that there is no simple equation that relates LNAPL thickness in a well to mobile LNAPL that has general applicability. In addition, not including entrapped and residual LNAPL led to a good estimate of the volume of LNAPL in Zone 2 but not a total LNAPL volume. API (2002) realized the presence of residual LNAPL (correlating to Zones 2, 3, and the vadose zone) by stating that the thickness of LNAPL in the formation is larger than the thickness in the well.

3.1.3 Experimental Design

Two experiments were performed to study the effects of water table fluctuations on LNAPL. The first experiment had no tidal cycles, barriers, or wells. This experiment served as a control. LNAPL was introduced on the left hand side of the tank and allowed to migrate across a 180 cm sand tank with no barriers. Details regarding materials and methods were previously presented in Sections 2.6 and 2.7. A total of 690 mL of diesel (herein referred to as LNAPL) were added to the tank at a rate of 6 mL/hr. The amount of LNAPL added was selected based on the amount needed to drive the LNAPL to the open water on the right hand side of the tank. When a sheen formed on the open water, the LNAPL feed was stopped and the amount of LNAPL delivered was recorded.

The second experiment was identical to the first, with the variation that the surface water levels were moved up and down by 22 cm every 12 hours. Two wells were placed in the tank to resolve the effect tides have on LNAPL thickness in a well versus the formation. In this experiment, 3.3 L of LNAPL was required (added at 6 mL/hr) to drive the LNAPL to the surface water section of the tank.

3.1.4 Results

3.1.4.1 Tidal Effects on LNAPL Distribution

A key observation of the experiment was that the initial invasion of LNAPL into unimpacted soils occurred as an intermediate phase along the top of the water capillary fringe. In a non-tidal system, the LNAPL body moved relatively quickly (as an intermediate wetting phase) towards the surface water. When the water table moved vertically, attributable to tidal fluctuations, LNAPL advancement was retarded as it was smeared vertically into Zones 1 and 3 (Figure 13 and Figure 14). The horizontal transport of LNAPL as an intermediate wetting phase was retarded due to LNAPL entrapment below the water table in Zone 1 as discontinuous blobs and ganglia. Residual LNAPL in Zone 3 and the vadose zone drained slowly, increasing the volume of LNAPL in Zones 2 and 3. At low tide, our experiments showed the majority of the LNAPL as a continuous phase in Zone 2, but some LNAPL was left in the Zone 3 (Figure 13). This was different than the reports by Marinelli and Durnford (1996) that stated at the historical low water level, all LNAPL is mobile while at high water level, all LNAPL is trapped as ganglia and blobs.

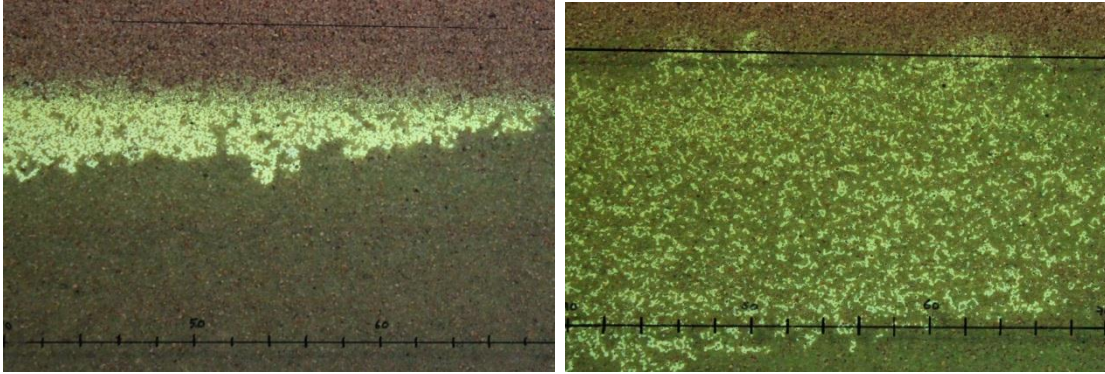


Figure 13. LNAPL distribution in non-tidal (left) and tidal (right) conditions at high tide (fluorescent green is LNAPL, dark green is water, no green is air).

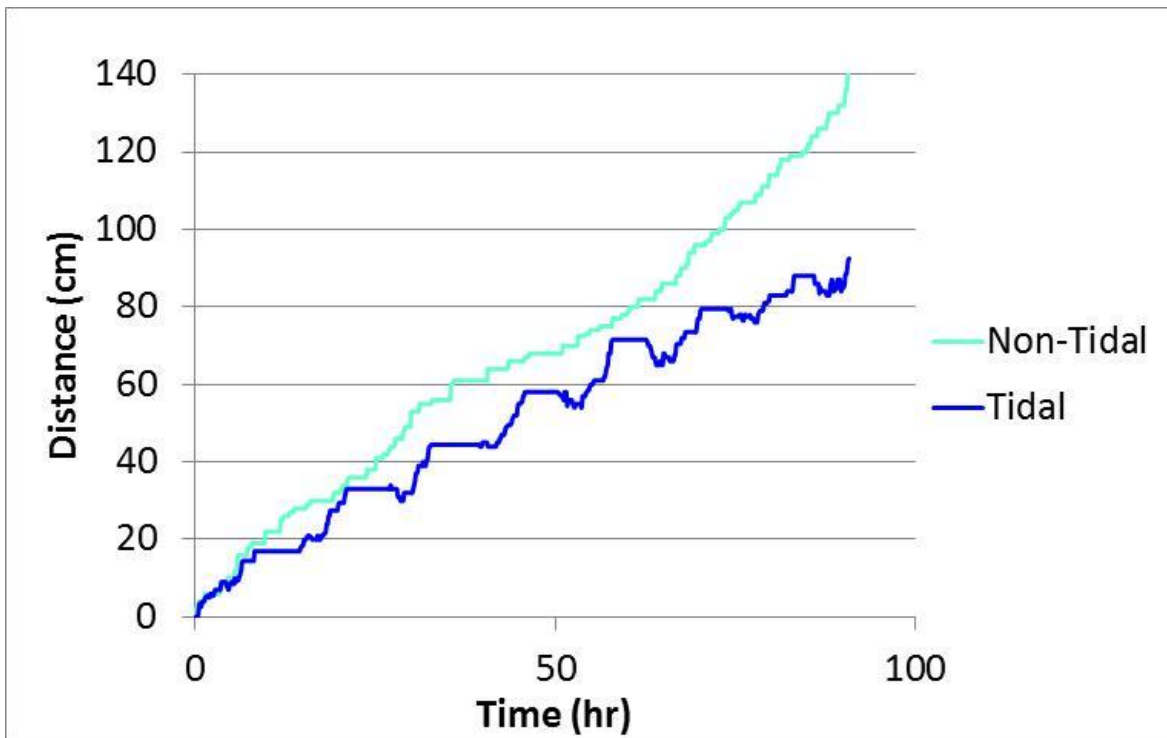


Figure 14. Comparison of LNAPL (leading edge) horizontal transport in tidal and non-tidal conditions.

The tidal experiments showed that LNAPL advances laterally predominantly during low water stages, given a continuous source of LNAPL. LNAPL movement primarily occurred in Zones 2 and 3. Figure 15 shows a graph of the horizontal movement of LNAPL versus time in the presence of fluctuating water levels. The graph indicates that at low stage, the LNAPL traveled

towards the GSI and at high stage the LNAPL mobility is reduced significantly. Furthermore, laboratory observations suggest, for the same quantity of LNAPL and the conditions of the experiment as described above, the LNAPL traveled 1.6 times further given non-tidal conditions. Note, the distance that the LNAPL will travel in porous media is dependent on characteristics of the fluid and media. This data supports the author’s hypothesis that water level fluctuations will retard LNAPL migration. Understanding LNAPL migration occurs at low water stages is important because it means that if the water level has been increased from storms or runoff, the majority of the LNAPL in the subsurface is immobile in Zone 1. However, if the water level is depressed from the installation of wells in the area, the size of Zone 1 will decrease and Zones 2 and 3 will increase. This results in more LNAPL being mobile than previously assumed.

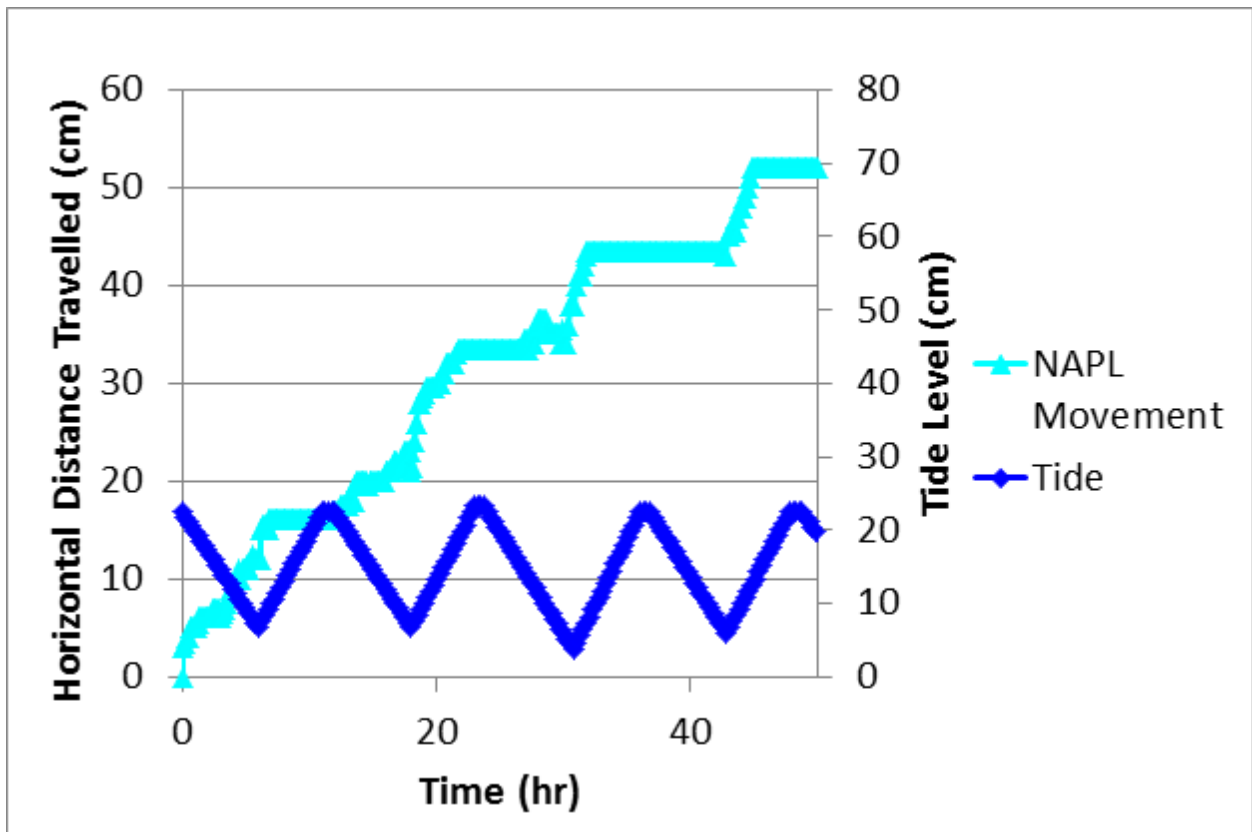


Figure 15. LNAPL transport in the presence of tidal cycles.

3.1.4.2 LNAPL Thickness in Wells versus Formation

A key observation of this experiment was the correlation between LNAPL thicknesses in wells versus the LNAPL thickness in Zone 2 and a lack of correlation to total LNAPL. An example of measured well thickness versus LNAPL in Zone 2 is shown in Figure 16. As observed in our experiments and commonly seen with field data, in-well LNAPL thicknesses increase with falling water levels and decrease with rising water levels (Figure 17). This confirms results by Marinelli and Durnford (1996), Kembrowski and Chiang (1990), and API (2002). The variation in thicknesses supports the idea that in order to create an equation correlating LNAPL thicknesses in wells to LNAPL in Zone 2, the system must be at vertical equilibrium. At vertical equilibrium, the LNAPL is immobile and the amount in each zone is constant. This results in the ability to create an equation that can describe the amount of LNAPL in Zone 2. When the system is not at vertical equilibrium, the variation in the thickness in the well versus Zone 2 is constantly changing and no simple equation can estimate the Zone 2 LNAPL. Note, the minimum LNAPL thickness in Figure 17 increases over time due to the overall increase of LNAPL in the tank.

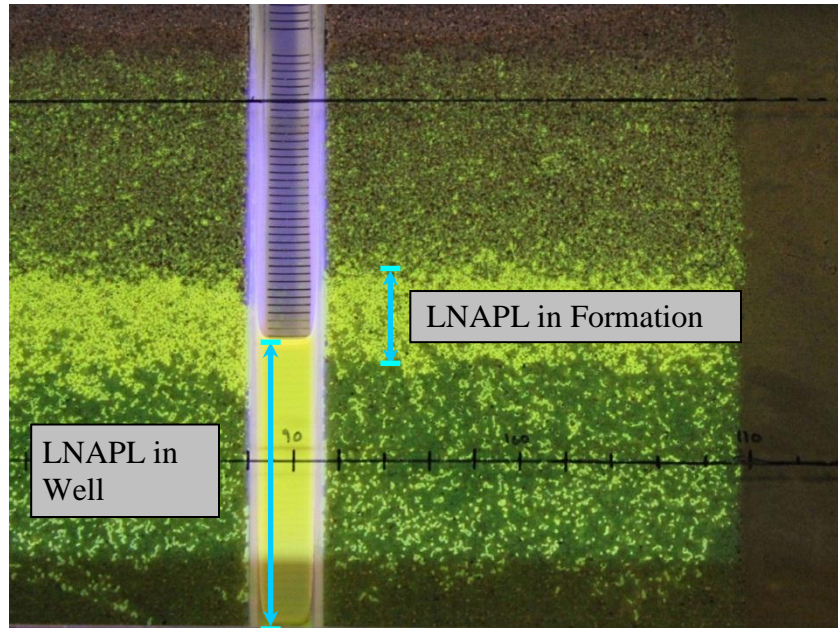


Figure 16. LNAPL thickness in well compared to thickness in formation.

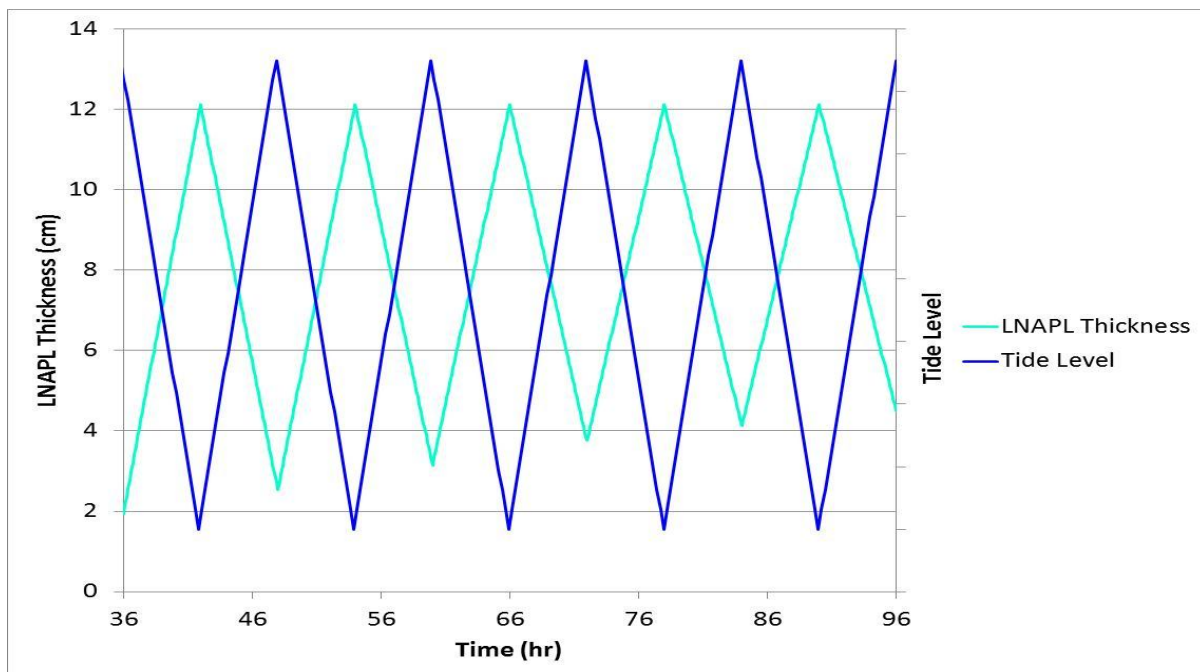


Figure 17. Relationship between LNAPL thickness and tidal level.

3.2 Capillary Barrier

Herein, capillary barriers are vertical walls of well-sorted fine-grained material with displacement pressures that are greater than the surrounding formation. In Zone 1, LNAPL

migration is limited by discontinuities of the LNAPL phase. Zone 2 LNAPL will not enter the capillary barrier as long as $P_c < P_d$. In Zone 3, the LNAPL is unable to migrate laterally because the capillary barrier has a higher capillary rise than the surrounding formation (Figure 18). Herein, the high capillary rise in the barrier will be referred to as a speed bump. The high capillary rise disrupts the elevation of the air-water interface. The LNAPL is unable to “jump” 4 cm vertically to overcome this speed bump, and, therefore, precluded in its migration. Further details regarding capillary barriers are presented in Section 3.2.2.



Figure 18. Capillary rise within a capillary barrier compared to the surrounding formation.

3.2.1 Objective

The objectives of the capillary barrier experiments presented in this subsection were to determine:

- The efficacy of using capillary barriers to control lateral migration of LNAPL
- The benefits of employing LNAPL recovery in conjunction with capillary barriers

3.2.2 Background

Following the volume balance presented in Section 2.1.4, altering the inflows and losses in a near-shore reference volume would assist in limiting LNAPL from appearing at GSIs. To reduce inflows and increase recovery, a capillary barrier and recovery well could be emplaced at a GSI. The capillary barrier, in theory, would preclude LNAPL migration and result in the build-up of LNAPL for increased recovery. LNAPL recovery would reduce the possibility of LNAPL outflow to surface water and increase the sustainability and longevity of the barrier.

Extensive research has been conducted with using horizontal capillary barriers to limit vertical flow of the wetting fluid (Shackelford et al., 1994, Parent and Cabral, 2005; Aubertin et al., 2009; Qian et al., 2009; McCartney and Zornberg, 2010; Zornberg et al., 2010). This research will be presented, however, the use of capillary barriers in the subsequent sections will be as vertical barriers that impede the advancement of nonwetting and intermediate wetting phases. Capillary barrier mechanisms for limiting migration for the wetting, intermediate wetting, and wetting phases are different for horizontal and vertical barriers.

A capillary barrier effect occurs when a fine-grained layer of media is on top of a coarse-grained layer of media (Shackelford et al., 1994, Parent and Cabral, 2005; McCartney and Zornberg, 2010; Zornberg et al., 2010). The capillary barrier effect restricts the downward flow of the wetting fluid and is due to the different relative permeabilities of the two layers. Thus, the capillary barrier effect causes water diversion and reduces the amount of infiltration resulting in their common use as landfill covers for waste disposal areas (Shackelford et al., 1994; Parent and Cabral, 2005; Aubertin et al., 2009; Qian et al., 2009).

For a vertical capillary barrier, the barrier is saturated with the wetting fluid. Corey (1986) states that the fine material for a capillary barrier must have a displacement pressure greater than the capillary pressure of the nonwetting fluid in order to prevent breakthrough of the nonwetting fluid. As a result, the LNAPL thickness in Zone 2 will increase.

The amount of LNAPL that can be removed depends on the amount of LNAPL that is present as a continuous phase (Zone 2 and 3) and can migrate to a well. Experiments by Marinelli and Durnford (1996) show that as the water table is lowered, more LNAPL is present as a continuous nonwetting phase, and, thus, recoverable. Schwille (1988) makes the same observation and adds that as the water table lowers, the LNAPL is allowed to infiltrate lower areas of the formation because the pores are gravity drained of water. As the water table is raised again, the LNAPL that penetrated deeper portions of the formation is likely to be entrapped as a discontinuous nonwetting phase in Zone 1.

Installing recovery wells will assist in LNAPL recovery. Water table fluctuations, however, will decrease recovery due to smearing of the LNAPL (Parker, 1989) into Zones 1 and 3. As the LNAPL initially enters the well, the thickness in the well reaches a critical thickness that is so small that the LNAPL is disconnected from the formation and immobile (Blunt et al., 1995). Generally, this occurs when the thickness of LNAPL in the well is insufficient to reach the necessary capillary pressure to connect the LNAPL in the well to the formation. No LNAPL can be recovered from the formation by pumping the well when P_c is less than P_d . However, if more LNAPL enters the well, the thickness increases and LNAPL will be recoverable.

3.2.3 Experimental Design

Two capillary barrier experiments were performed. The first experiment had a single fully penetrating, 4 cm wide, vertical capillary barrier on the right hand side of the tank and no wells. Tidal cycles were imposed throughout the experiment. Tidal cycles consisted of the water table moving up and down by 22 cm every 12 hours. The amount of LNAPL added, 3.3 L at 6 mL/hr, was based on the amount required for the LNAPL to migrate from the left hand side of the tank, past the capillary barrier, and reach the open water.

The second capillary barrier experiment was identical to the first with the addition of two wells emplaced in the tank (Figure 19) and the amount of LNAPL fed into the tank. The capillary barrier was placed to the right of the second well to prevent LNAPL migration. The duration of the experiment was 5 months. A total of 2.5 L of LNAPL, a fixed amount, was fed into the tank over the first 17 days. Next, the LNAPL release was stopped, and LNAPL was removed at low tide by using a peristaltic pump. The depth at which pumping occurred was adjusted manually to ensure only LNAPL was recovered. Table 5 shows the characteristics of the capillary barrier experiments.

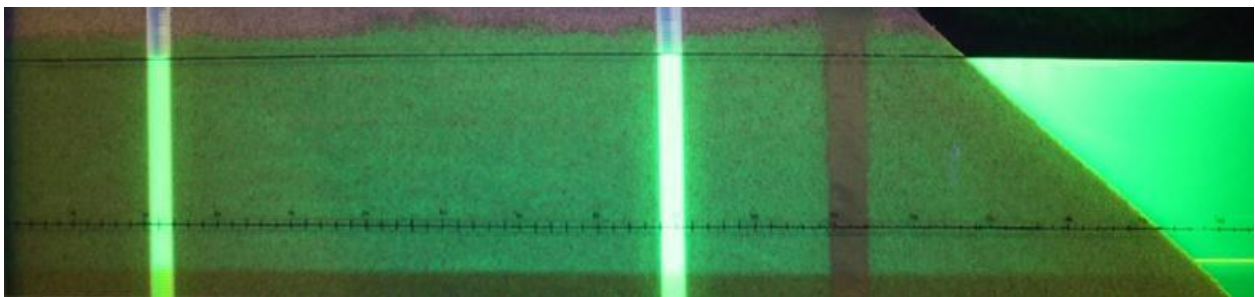


Figure 19. Capillary barrier experiment with two wells and a capillary barrier.

Table 5. Characteristics of barrier experiments.

Experiment	Number of			LNAPL added (L)
	Cap. Bar.	Org. Bar.	Wells	
Capillary Barrier 1	1	-	-	3.3
Capillary Barrier 2	1	-	2	2.5
Organoclay Barrier 1	-	1	-	2.3
Organoclay Barrier 2	-	2	-	2.7

3.2.4 Results

3.2.4.1 Capillary Barrier Efficacy

A key observation of this experiment was that capillary barriers are an effective method to preclude LNAPL migration so long as the capacities of the barrier to limit Zone 2 and 3 LNAPL migration are not exceeded. An application of a capillary barrier to limit lateral migration of LNAPL is depicted in Figure 20. The figure shows the capillary barrier and LNAPL build-up in Zone 2 just prior to failure. The build-up of LNAPL in Zone 2 occurred because $P_c < P_d$ and the speed bump created by the high capillary rise in the barrier was sufficiently large to limit overtopping. The LNAPL in Zone 1 did not penetrate the barrier because it was immobile as a discontinuous phase. Failure of the barrier was due to LNAPL going over and under the barrier, triggered by massive build-up of LNAPL in Zone 2 and limitations of the tank.

The graph in Figure 20 shows the saturation curve that corresponds to the photograph. As can be seen in the graph, there is a ten centimeter portion of media that has a saturation around 0.95-0.98. This is easily discernible in the photograph. This highly saturated area corresponds to Zone 2 and shows the ability of the capillary barrier to preclude LNAPL migration. The minor saturation at the top of the photograph and in the graph corresponds to the LNAPL in Zone 3 and

the vadose zone. Concurrently, the saturation at the bottom of the photograph and in the graph represents the LNAPL in Zone 1.

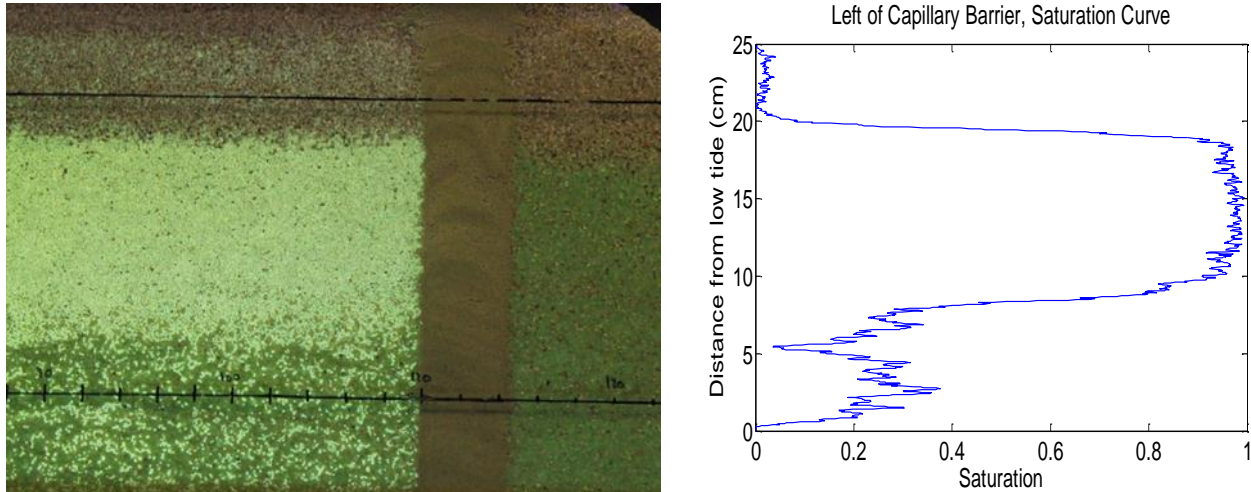


Figure 20. LNAPL build-up due to capillary barrier and corresponding saturation curve obtained from transformation of the digital image to LNAPL saturation.

The massive amount of build-up prior to failure prompted the question, “How much LNAPL can be recovered with a capillary barrier present?” This led to the second capillary barrier experiment with LNAPL recovery.

3.2.4.2 Capillary Barrier with LNAPL Recovery

A key observation of this experiment was that the conjunctive use of a capillary barrier and a LNAPL recovery well is a promising strategy to sustain performance of a capillary barrier at a GSI. Recovery began after 2.5 L of LNAPL was added and LNAPL had accumulated in Zone 2 and wells. Over a period of 25 days, 2.1 L (84% of total) of LNAPL was recovered. After 8 weeks, no more LNAPL could be removed though residual was observed in Zone 1, 3, and the vadose zone. To mobilize entrapped LNAPL, the low tide was lowered by 4 cm and tidal cycles continued. After 3 weeks, an additional 1.6 mL, or 0.064%, was recovered. The vertical

smearing of LNAPL and residual in Zone 1 decreased potential recovery rates. Therefore, water table fluctuations were stopped at low stage and the LNAPL in the vadose zone was allowed to drain and migrate towards the wells. Lowering the water table, and allowing the tank to reach equilibrium, caused the entrapped LNAPL in Zone 1 to become mobile, migrate to a well, and increase recovery. Over 10 weeks an additional 200 mL, or 8%, was removed. In total, 92% of the released LNAPL was recovered. This illustrates how water levels can be manipulated to optimize LNAPL recovery. In addition, the experiment demonstrated the efficacy of capillary barriers used in conjunction with LNAPL recovery. During each of the recovery phases, it was noted that the amount of LNAPL removed approached an asymptote (Figure 21). Altering the water levels allowed a new asymptote to be approached. This brings up the question of when is it no longer feasible to recover LNAPL (Sale and Applegate, 1997). It should be noted that LNAPL recovery was performed in an idealized tank, with homogeneous and isotropic material, which is not representative of field conditions.

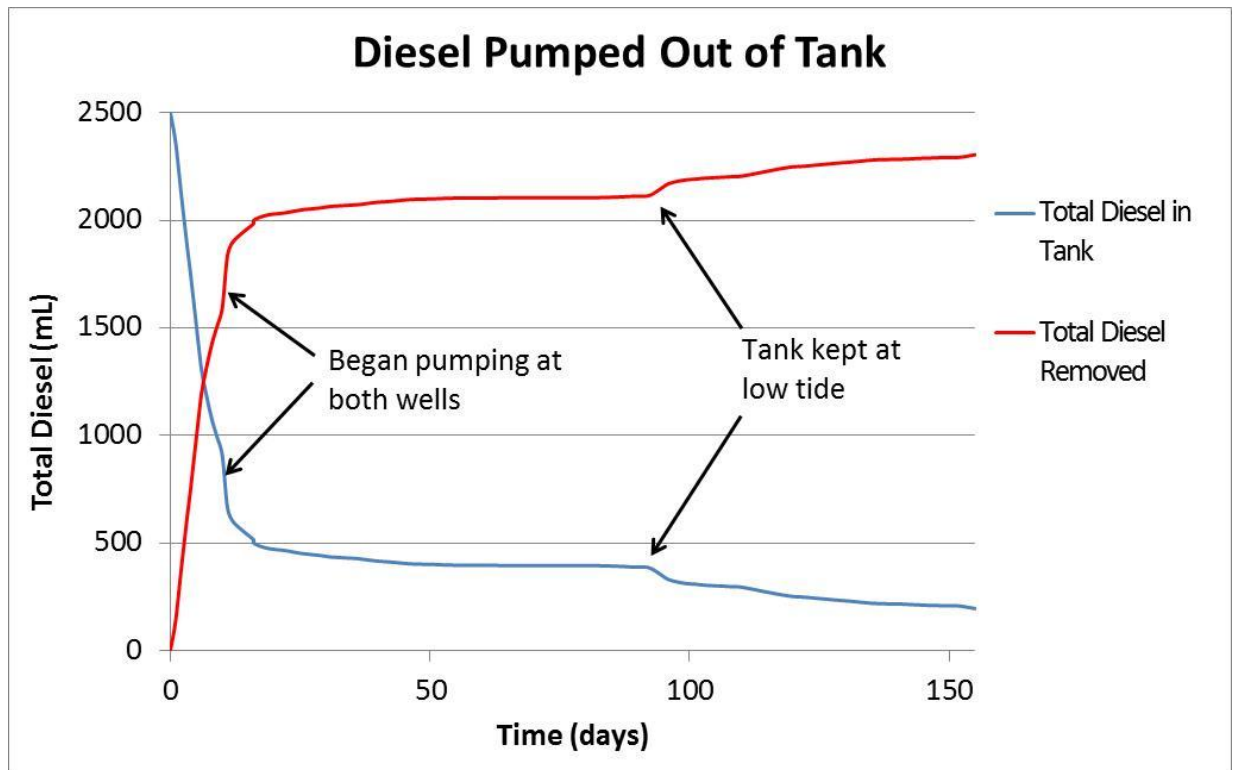


Figure 21. Graph of LNAPL (diesel) recovered in the capillary barrier with recovery experiment.

Analysis of the results suggests low water levels can mobilize trapped residual LNAPL in Zone 1. Pumping at low tide after these periods of LNAPL mobilization can increase total LNAPL recovery. As LNAPL was removed from the tank, the relative saturation decreased creating discontinuities in the LNAPL. These discontinuities result in making it more difficult to mobilize ganglia and blobs. Currently, there is no effective way to completely remove 100% of LNAPL at a site using pumping.

The supplemental materials section contains a link to the capillary barrier video which shows this experiment. The video includes the LNAPL migration, build-up, and removal.

3.3 Organoclay Barrier

Herein, organoclay barriers are vertical walls of mixtures of well-sorted organoclay and sand that reduce LNAPL migration by sorption. Unlike sand in capillary barriers, organoclay is hydrophobic. Hydrophobicity has the effect of depressing the capillary fringe to levels lower than the capillary fringe in the adjacent formation (Figure 22). The depressed capillary fringe creates a topographic trough that draws LNAPL in to the barrier via Zone 3. With time, inflow of LNAPL via Zone 3 leads to the formation of Zone 2 LNAPL in the barrier. LNAPL in Zone 1 will be precluded from entering the barrier due to the discontinuous nature of LNAPL in Zone 1. Further details regarding organoclay barriers are presented in Section 3.3.2.

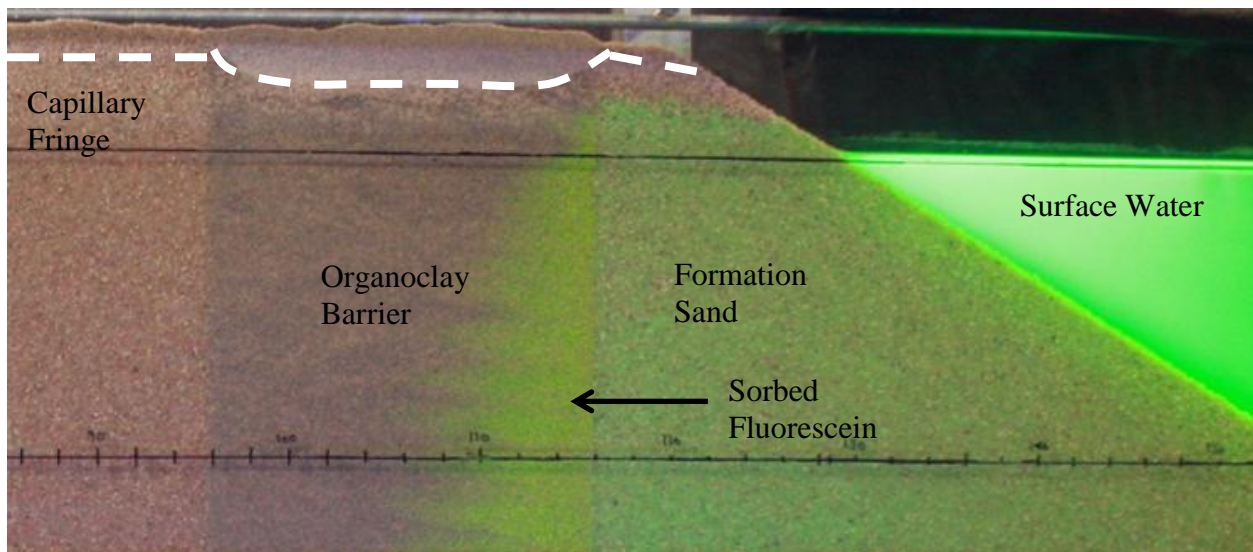


Figure 22. Depressed capillary rise in organoclay barrier compared to the formation.

3.3.1 Objective

The objectives of the organoclay barrier experiments were to determine:

- The efficacy of using organoclay barriers to limit LNAPL migration

- The efficacy of adding baffles and/or coarse-grained sand layers (drains) to an organoclay barrier

3.3.2 Background

Organoclay barriers have been used to control LNAPLs at GSIs (i.e. Chevron's refinery in Burnaby, British Columbia, Canada). Organoclay barriers work on the principle of increasing the storage capacity of a near-shore element (REV_{cap}) by sorption. For sorption to be efficient, LNAPL in Zones 2 and 3 must be able to enter the barrier, make contact with the organoclay, and sorb.

Organoclay is clay that is altered to be hydrophobic and oleophilic. The clay is modified by replacing the inorganic cations in the clay by quaternary amines (Lo, 2001; Gullick and Weber, 2001; Voudrias, 2002; Lee et al., 2012). Once organoclay has been altered, it will swell when in contact with LNAPLs, unlike natural clays which swell when in contact with water (Lo and Yang, 2001a). Organoclay barriers are commonly used as liners at waste sites. Requirements for liners at waste sites are based on a low hydraulic conductivity (USEPA, 1989); therefore, swelling of the barrier to lower the hydraulic conductivity is seen as a positive. Bentonite has a large swelling capacity and is often mixed with organoclay to be used as a barrier or liner for waste sites (Lo, 2001; Gullick and Weber, 2001; Voudrias, 2002).

Lower hydraulic gradients will decrease the advective flow of contaminants but diffusion may still exist (Gullick and Weber, 2001; Lo and Yang, 2001a; Voudrias, 2002). Research has shown that contaminant flux is often lower than water flux (Lo and Yang, 2001b; Mahler et al., 2011). Organoclay will further decrease the contaminant flux due to sorption (Lo and Yang, 2001b; Gullick and Weber, 2002). Voudrias (2002) expands on this lower flux and states that once

sorbed to the organoclay, it can be held in place for biological degradation or chemical decay. A drawback of organoclay barriers is that sorbed LNAPL may become a long-term source of dissolved phase contaminants if the barrier is not removed after remediation is complete (Lee et al., 2012).

3.3.3 Experimental Design

Two organoclay barrier experiments were performed. The first experiment contained a vertical 20 cm wide organoclay barrier on the right hand side of the tank that fully penetrated the sand (see Figure 8, Section 2.2.2.1). Prior to the addition of the LNAPL, the tank was fully saturated with water. This created a water wet media. Tidal cycles were present throughout the experiment and had a 22 cm range from high to low tide every 12 hours. A total of 2.3 L of LNAPL were delivered into the tank. The amount of LNAPL was based on the amount required to cause the organoclay barrier to fail. Failure was defined as LNAPL being observed on the down-gradient side of the barrier.

The second organoclay barrier experiment contained two organoclay barriers (Figure 23). The first barrier was 15 cm wide and contained three HDPE baffles to prevent overtopping. The second organoclay barrier was 20 cm wide with four organoclay and three coarse sand layers. Tidal cycles were identical to the first organoclay barrier experiment. In total, 2.7 L of LNAPL were added to the tank. This volume was based on the amount of LNAPL needed for both barriers to fail. Characteristics of both organoclay experiments are given in Table 5 (shown in Section 3.2.3).

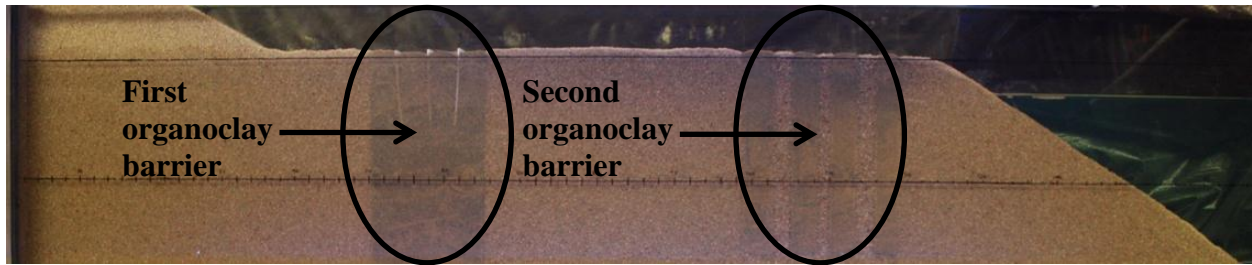


Figure 23. Second organoclay experiment with HDPE baffles and coarse-grained drains.

3.3.4 Results

3.3.4.1 Organoclay Barrier Efficacy

Key observations of this experiment were rapid failure of the organoclay barrier through Zone 3 and non-uniform contact of LNAPL with the organoclay in the barrier. Initially, as the LNAPL made contact with the barrier, the LNAPL in Zones 2 and 3 was unable to enter the barrier due to water in the pores. The water was present in the pores of the organoclay barrier due to slow drainage, not capillary rise. The LNAPL in Zone 1 was discontinuous and immobile. As the LNAPL continued to enter the tank, the LNAPL became thick enough in Zone 2 and 3 to reach a height to fill the depression (created by the depressed capillary fringe) in the organoclay barrier. As the LNAPL reached this height, it was able to enter the barrier and resulted in overtopping (Figure 24, left). The average saturation corresponding to the overtopping (Figure 24, right) is approximately 4%.

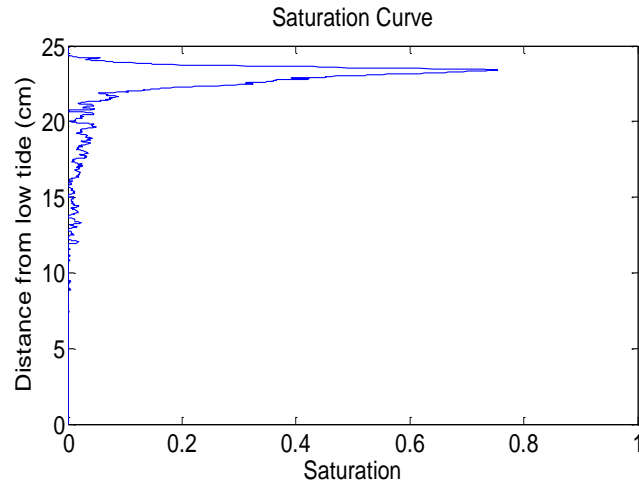
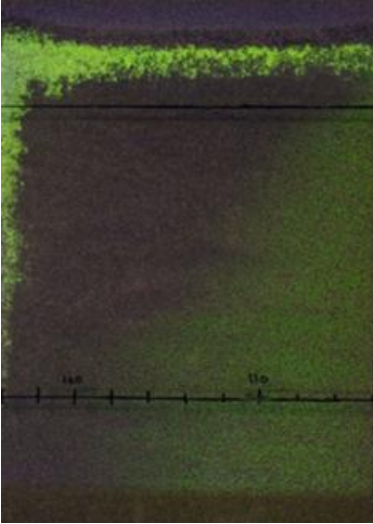


Figure 24. First organoclay barrier experiment showing overtopping and the corresponding saturation curve obtained from transformation of the digital image to LNAPL saturation.

As more LNAPL migrated to the barrier, the LNAPL continued to travel along the depressed capillary fringe. As the water level fell, the water in the organoclay drained. Thereafter, the LNAPL that had travelled across the top of the barrier drained down through the barrier causing preferential flow paths. These flow paths led to an early failure and little sorption. Figure 25 shows the preferential flow of LNAPL through the barrier and the average saturation at failure. Average saturation at failure was approximately 11%, which is much lower than anticipated and thus deemed an early failure. A link to the video of this experiment can be found in the supplemental materials section.

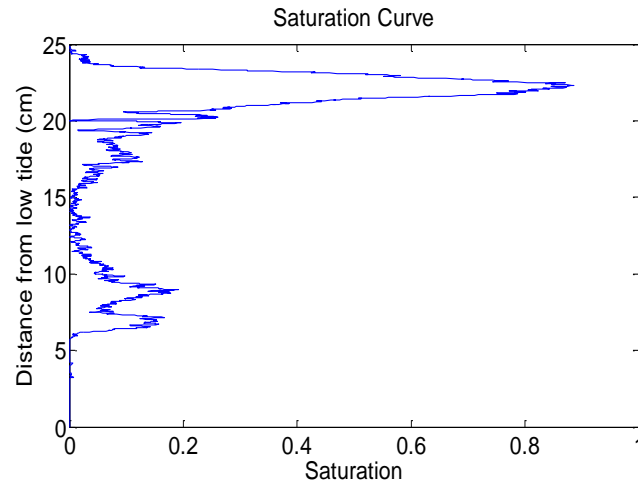
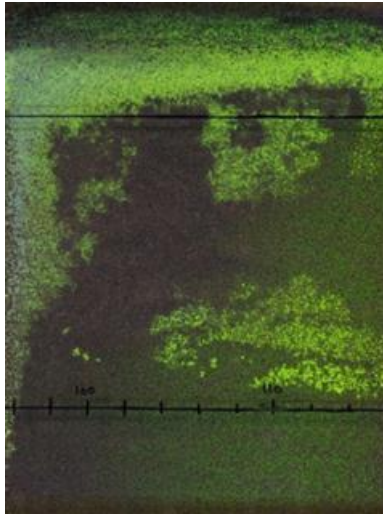


Figure 25. First organoclay barrier experiment at failure, showing preferential flow and the corresponding saturation curve obtained from transformation of the digital image to LNAPL saturation.

An additional observation made during cleaning the tank between experiments was that the organoclay had swelled. Swelling made it difficult to remove the barrier and raised the idea that it may be difficult to excavate in the field. This may reduce the efficacy of using an organoclay barrier.

3.3.4.2 Baffles and Drains as Enhancements to an Organoclay Barrier

A key observation of this experiment was that simple improvements, such as inserting baffles or coarse-grained drains, to the organoclay barrier can greatly enhance LNAPL bulk sorption prior to failure. Figure 26 shows the first organoclay barrier (three HDPE baffles) at failure and the corresponding saturation curve. The average saturation was approximately 43% at failure, which is four times more sorption than with no baffles present. Sorption was increased because the baffles resulted in the LNAPL in Zone 2 building-up pressure to overcome the displacement

pressure. As a result, the LNAPL moved through the barrier rather than across the top of the barrier.

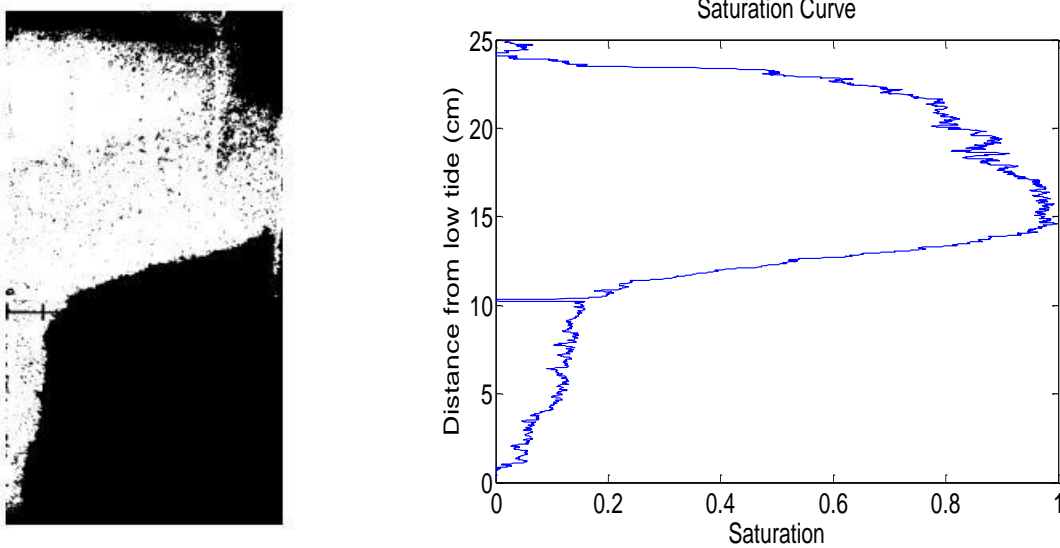


Figure 26. First barrier in second organoclay experiment, with 3 HDPE baffles, at failure and the corresponding saturation curve obtained from transformation of the digital image to LNAPL saturation.

During the experiment, it was noted that failure of the barrier happened prior to full saturation. The saturation could have been increased if the baffles were deeper or if there was a baffle on the edge of the organoclay. Longer baffles that went deeper into the barrier would have caused the LNAPL to migrate deeper in the barrier for sorption. This would have increased the overall sorption of the barrier prior to failure. The sorption on the right side of the barrier was lower because LNAPL was not forced upwards prior to exiting into the formation. A fourth baffle, at the edge of the organoclay barrier, may have inhibited the migration and allowed for increased sorption prior to failure.

Figure 27 shows the second organoclay barrier (drains) at failure. The average saturation of the second barrier was approximately 34% at failure, which is 3 times more saturated than the original organoclay barrier. The drains increased water drainage in the organoclay and decreased the time it took for Zone 3 to form in the barrier. Once Zone 3 formed, LNAPL could migrate into the barrier and sorb to the organoclay.

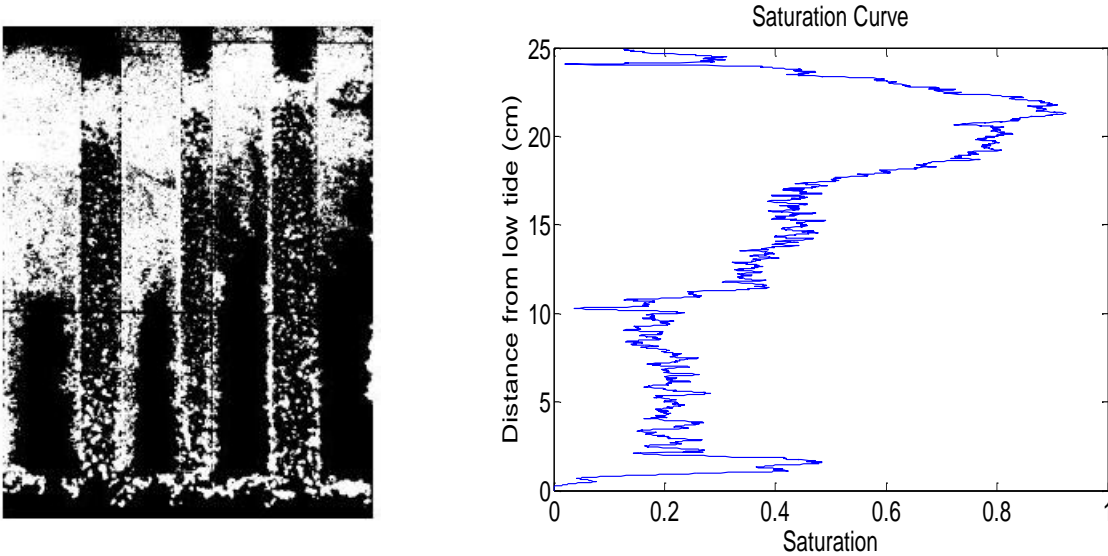


Figure 27. Second barrier in second organoclay experiment, with drains, at failure and the corresponding saturation curve for second barrier obtained from transformation of the digital image to LNAPL saturation.

Sorption in the second barrier could be increased with further improvements. It was observed that the coarse sand along the bottom of the barrier created its own preferential pathway. Failure of the barrier occurred due to LNAPL migrating through the sand, under the organoclay, and out of the barrier. Having the last organoclay segment go to the bottom of the tank, or at least deeper than the coarse sand, may have allowed more LNAPL to sorb prior to failure.

The simple changes made to the barriers and the large increase in saturation show that organoclay barriers can be an effective barrier if properly installed. Installation may be more

difficult with the second barrier (coarse-grained drains) than the first (baffles) but these are all considerations that must be taken into account when determining the proper remediation technique. A link to the video of this experiment showing both improved barriers is supplied in the supplemental materials section.

3.4 Conclusion

This chapter covered six sand tank experiments that looked at the influence of tidal cycles and the efficacy of capillary and organoclay barriers to limit LNAPL migration. Important conclusions from the experiments include:

- Initially, LNAPL invaded porous media along the top of the capillary fringe as an intermediate wetting fluid
- Water table fluctuations attenuated the migration of LNAPL due to smearing and entrapment
- Minimizing the size of Zone 1 (low water stage) has the potential to maximize LNAPL recovery
- LNAPL thicknesses in wells followed the overall fraction of LNAPL in Zone 2 which varies as a function of water levels
- Capillary barriers limit LNAPL migration by two processes
 - Zone 2 LNAPL is precluded from entering the barrier so long as $P_c < P_d$
 - Zone 3 LNAPL does not enter the barrier because of the high capillary rise, creating a speed bump, within the barrier
- Preferential flow of LNAPL through organoclay barriers can limit their effectiveness due in part to a capillary fringe depression in the barrier

- Organoclay barriers have limitations when used vertically; these limitations include preferential flow, slow drainage, and low overall sorption
- High-density polyethylene baffles can limit overtopping in an organoclay barrier and increased bulk LNAPL sorption in the organoclay barrier
- Coarse-grained sand layers (drains) interspersed in an organoclay barrier increased drainage and sorption of LNAPL

4. FORCE BALANCE APPROACH TO A SATURATION MODEL

Numerous empirical models have been developed to predict fluid saturations as a function of capillary pressure and porous media properties. This chapter reviews the most promising models. Building on work by others, an alternative approach is explored. The alternative approach considers the spreading coefficient and gravity as governing factors. For simplicity, the force balance approach neglects hysteresis, entrapped fluid, and residual fluid. The author acknowledges that hysteresis, entrapment, and residual can be important factors that deserve further attention. The model is applied to two and three-phase systems. Furthermore, the model is compared to the Brooks-Corey model (Brooks and Corey, 1964). The chapter closes with conclusions regarding the merits and limitations of the force balance approach.

4.1 Literature Review

Historically, fluid saturations in granular porous media have received broad attention in the fields of agronomy and oil and gas production. The following presents historical work as a foundation for exploring the feasibility of developing a fluid saturation model based on a force balance. Historical work presented will focus on two common two-phase models, a three-phase model, the importance of using interfacial tensions in models, and a model that utilizes the spreading coefficient.

4.1.1 Two-Phase Models

Two of the most common two-phase fluid saturation versus capillary pressure models are the Brooks-Corey (Brooks and Corey, 1964) and van Genuchten (van Genuchten, 1980) models. Both of these models are empirical as opposed to being based on physics. The Brooks-Corey model describes relationships between fluid saturations and capillary pressures in terms of a

bubbling pressure (P_b) and a pore size distribution index (λ , [dimensionless]). The bubbling pressure is the capillary pressure at which air flow is first observed. This is similar to the entry and displacement pressure. The pore size distribution index is a measure of the uniformity of the pore sizes in the media. An assumption of the Brooks-Corey model is that both fluid phases are continuous (Brooks and Corey, 1964). Building on work described by Burdine (1952), the Brooks-Corey model can also be used to estimate relative permeabilities for wetting and nonwetting phases. Equations for relative permeabilities described by Brooks and Corey will not be considered in this thesis. The Brooks-Corey model relies on the idea of an effective wetting phase saturation defined as:

$$S_e = \frac{S - S_r}{1 - S_r} \quad (10)$$

where S_r is the residual saturation [dimensionless]. The effective saturation is also defined in regards to the bubbling pressure and the capillary pressure (Brooks and Corey, 1964):

$$S_e = \left(\frac{P_b}{P_c}\right)^\lambda \quad \text{for} \quad P_c \geq P_b \quad (11)$$

Both P_b and λ are determined by plotting $\log S_e$ as a function of P_c/γ (for more information see Brooks and Corey, 1964). Note, Equation (11) is only applicable for $P_c \geq P_b$. For $P_c < P_b$, $S_e = 1$. This condition creates a discontinuous function.

The van Genuchten model gives relationships between saturation and capillary pressure in terms of constants and capillary head. Similar to Brooks and Corey, van Genuchten determined a method to estimate relative permeabilities of the wetting and nonwetting phases. However, van Genuchten built on work performed by Mualem (1976). The van Genuchten model describes the effective wetting phase saturation as:

$$S_e = \left(\frac{1}{1+(\alpha h)^n} \right)^m \quad (12)$$

where α [1/L] and n [dimensionless] are constants that depend on characteristics of the porous material, $m = 1 - 1/n$ [dimensionless], and h is the capillary head [L] (van Genuchten, 1980). Another difference in the two models is that the van Genuchten model assumes that $S_e > 0$ for any $P_c > 0$. This means that the van Genuchten equation assumes a zero displacement pressure for all porous media and forms a continuous function. It is possible to choose values of α , n , and m that allow for the van Genuchten model to closely resemble the Brooks-Corey model, except for at low capillary pressures. A drawback of these models is that neither model accounts for hysteresis, which can alter the residual and overall saturation in the porous media. Note, in some computer models, hysteresis can be accounted for in these models by running the equation twice. Parameters are set for imbibition curves on one run and drainage curves on the second.

4.1.2 Three-Phase Model

In general, analyses of three-phase systems are far more complex than two-phase systems. A common example of a three-phase system is a petroleum reservoir containing water, oil, and gas. Most three-phase models are built on existing two-phase models. The ability to build a three-phase model accurately from a two-phase model is based on the Leverett concept (Leverett, 1940). Parker and Lenhard (1987) created a model for fluid saturations versus capillary pressure relations in a three-phase system that takes into account hysteresis and entrapped fluids. Two years later they modified their model (Lenhard et al., 1989) so that it also considers non-drainable LNAPL, otherwise known as residual LNAPL. The formulas they described build on the van Genuchten model, use saturations measured during imbibition and drainage cycles, and have a scaling factor, β [dimensionless]. The scaling factor is a ratio of interfacial tensions

between liquids. The model created is relatively complete because it takes into account hysteresis, entrapment, and residual LNAPL. Thus, it looks at the total LNAPL in the porous media and not just the LNAPL in Zone 2. Not accounting for entrapped and residual LNAPL in Zones 1 and 3 can drastically change the saturation curves. In addition, the entrapped and residual LNAPL can be a source of future aqueous or vapor contamination. For more information regarding the model and the complex equations see Parker and Lenhard (1987) and Lenhard et al. (1989).

4.1.3 Importance of Interfacial Tensions

Scaling factors based on interfacial tensions have been used in multiple models (Parker and Lenhard, 1987; Cary et al., 1989; Blunt et al., 1995; and Oostrom et al., 2003). These authors all realize the importance of the difference in interfacial tensions of the fluids and the need to incorporate them into their models but none of them use the spreading coefficient. As previously defined, the spreading coefficient equals:

$$S_c = \sigma_{aw} - (\sigma_{ao} + \sigma_{ow}) \quad (1)$$

In this system it is assumed that the order of wetting to porous media is water > LNAPL > air.

The ability to spread can also be related to the contact angle, known as Young's equation.

Young's equation is usually used for vapor-liquid-solid systems (Young, 1805) and is defined as:

$$\sigma_{aw} * \cos \theta = \sigma_{as} - \sigma_{ws} \quad (13)$$

where the subscript s represents the solid, θ is the contact angle [°], and other variables are as previously defined. The contact angle is the angle that is formed by the intermediate wetting phase between the other two substances (Young, 1805) as shown in Figure 28. The closer the

angle is to zero, the greater the spontaneity of the intermediate wetting phase to spread. When the contact angle is zero, the liquid is considered completely spreading and covers the entire solid surface (Bernett and Zisman, 1968; van Oss et al., 1992).

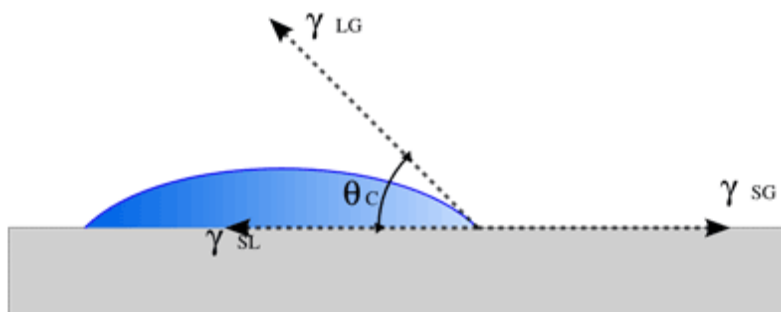


Figure 28. Contact angle for a gas-liquid-solid system.

Calculating the spreading coefficient reveals important information regarding the LNAPL's ability to migrate in Zone 3. Spreading coefficients are based on the interfacial tensions of the fluids. As two fluids remain in contact with each other, molecules of one fluid will dissolve into the adjacent fluid and vice versa. Correspondingly, over time, the interfacial tension between two fluids can change and result in an increase or decrease in the spreading coefficient (Schroth et al., 1995; McBride et al., 1992; Keller et al., 1997; Oostrom et al., 2003). As the spreading coefficient decreases, the liquid is less spontaneous in its spreading ability.

The sign of the spreading coefficient is significant because it influences the lateral extent of the plume and the residual content. A positive spreading coefficient (spreading liquid) means that the liquid will spontaneously spread and a negative spreading coefficient (non-spreading liquid) means the liquid will contract and form lenses (Vizika and Lombard, 1996). Liquids with positive spreading coefficients tend to have a larger lateral LNAPL plume extent than liquids with negative spreading coefficients. In addition, non-spreading liquids have a higher residual LNAPL saturation in the vadose zone due to the liquid breaking into isolated ganglia and blobs

(Schroth et al., 1995; Kalaydjian and Tixier, 1991; Oostrom et al., 2003). As the spreading coefficient decreases, the residual of non-spreading liquids increases (Chatzis et al., 1988 as cited by Hofstee et al., 1997).

To build an accurate three-phase model, the Leverett concept must be tested for spreading and non-spreading liquids. It was found that the Leverett concept does not apply for non-spreading liquids (Hofstee et al., 1997; Oostrom et al., 2003) because the discontinuities make it difficult to apply continuous two-phase equations.

4.1.4 Use of Spreading Coefficient

The use of the spreading coefficient in saturation models is limited. The only model found by the author that uses the spreading coefficient was developed by Schroth et al. (1995). Schroth et al. built on a model by Pantazidou and Sitar (1993) to determine the thickness of an LNAPL lens. Pantazidou and Sitar determined the thickness of an oil lens in the formation can be calculated by:

$$T = \frac{1}{\rho_o * g} * \left(\frac{4 * (\sigma_{ow} + \sigma_{oa})}{d_n} - \rho_w * g * h_w \right) \quad (14)$$

where:

d_n = pore neck diameter [L]

ρ = density of the phase (o for LNAPL and w for water) [M/L^3]

g = gravity [M/T^2]

h_w = height of the lens above the water table [L]

Schroth alters the equation for thickness by substituting equations for the pore neck diameter and the height of the lens above the water table into Equation (14):

$$d_n = \frac{4*\sigma_{aw}}{\rho_w*g*h_{cap}} \quad (15)$$

where h_{cap} is the capillary fringe height [L] and all other variables are as previously defined.

$$h_w = h_{cap} - T \quad (16)$$

Resulting in a new equation for the lens thickness:

$$T = \frac{4*(\sigma_{aw}-\sigma_{ao}-\sigma_{ow})}{d_n*g*(\rho_w-\rho_o)} \quad (17)$$

Schroth et al.'s equation, after the substitution, includes the spreading coefficient; however, when a fluid has a negative spreading coefficient the thickness is also negative. It is not possible to have a negative thickness; therefore, Equation (17) has limited use. No other models have been found by the author that utilizes the spreading coefficient.

4.2 Force Balance Model

This section describes a model developed based on a force balance approach. This section includes information regarding the scenario considered, a force balance, and solutions for the intermediate wetting, wetting, and nonwetting phase saturations.

4.2.1 Scenario and Assumptions

The model considers a three-phase system consisting of air, LNAPL, and water at equilibrium. The model evaluates fluid saturations versus elevation above a datum. The LNAPL considered herein is diesel. The LNAPL is introduced as an intermediate wetting fluid to the system at the

air-water interface. Air is considered the nonwetting phase and water the wetting phase. The water table is held at a fixed elevation. The porous media is uniformly packed and water wet. Initially, the media is fully saturated with water. Subsequently, the water is allowed to drain. Lastly, LNAPL is added. With this scenario, water is on a drainage cycle and LNAPL is on an imbibition cycle. The author understands that the saturation of LNAPL would be different for imbibition and drainage cycles. When analyzing the force balance, it is assumed that the water coats every sand particle and that the sand and water are one phase (per conversations with Art Corey, Emeritus Faculty, Colorado State University, 2012). For simplicity, the author is looking at a system where the LNAPL is on its first imbibition cycle; thus, it is not necessary to consider the effects of hysteresis. Constants in the model were experimentally evaluated and compared with published data, when available (Table 6). Methods were previously described in Section 2.2.3.3. The types of media shown refer to the assumed scenario for the model (named Model 1) and three types of media used for comparison in subsequent sections.

Table 6. Properties of media.

	S_c (dyne/cm)	ϕ	ρ_{iw}^c gm/cm ³	ρ_w^c gm/cm ³	r (mm)	P_b / γ (cm)	S_r	λ	ϕ_e
Model 1 ^a	13.2	0.41	0.828	1.0	1.37	-	-	-	-
Fine Sand ^b	55.0	0.377	1.0	-	-	41.0	0.167	3.70	0.314
Volcanic Sand ^b	55.0	0.351	1.0	-	-	16.0	0.157	2.29	0.296
Glass Beads ^b	55.0	0.370	1.0	-	-	29.0	0.085	7.30	0.338

^a experimentally evaluated by the author

^b except as otherwise noted, values are from Brooks and Corey 1964

^c subscripts iw are for the intermediate wetting fluid and w is for the wetting fluid

^d estimated based on work by Jańczuk et al., 1984

4.2.2 Force Balance

When looking at a vertical profile of fluid saturations and the forces affecting fluid saturations, there are two main forces. The force acting in the up direction is the spreading force, which is

based on the spreading coefficient acting at the three-phase interface. The force acting in the down direction is the gravity force. There is no friction force because the system is under hydrostatic conditions. All forces are cast in terms of force per horizontal area of porous media.

4.2.2.1 Spreading Force

The spreading force is based on the spreading coefficient assuming the contact angle of the wetting phase is effectively zero. Figure 29 shows a sand grain in a representative elementary volume (REV) and liquid wicking half-way up a sand grain. Wicking is deemed the spontaneous movement of the liquid in the up direction in porous media. In Figure 29, the spreading force will act along the wetted perimeter of the sand grain, where wicking stopped and the three-phase interface exists. The wetted perimeter is given by:

$$Wp = \int_0^r 2 * \pi * z * dz \quad (18)$$

$$Wp = \pi * r^2 \quad (19)$$

where r is the radius of the sand grain [L]. The spreading force per area, F_s , will then equal the spreading coefficient multiplied by the wetted perimeter, divided by the horizontal area of the REV [L²]. This leads to:

$$F_s = S_c * \frac{\pi * r}{(2 * r)^2} = S_c * \frac{\pi * r}{4 * r^2} = S_c * \frac{\pi}{4 * r} \quad (20)$$

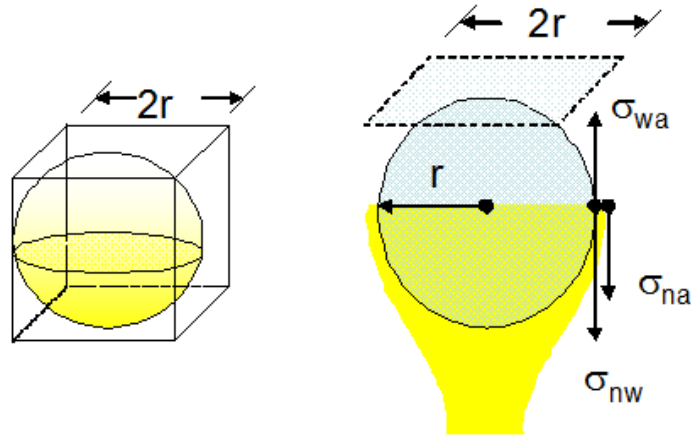


Figure 29. Sand grain in an REV and LNAPL wicking up a sand grain.

4.2.2.2 Gravity Force

A gravitational force is mass (m) of LNAPL per horizontal area of porous media times the gravitational constant (g). The force will act at any point that has a mass. The LNAPL mass in the REV will equal:

$$m = S_n * \rho_n * A * b * \Phi \quad (21)$$

where S_n is the LNAPL saturation [dimensionless], A is the cross sectional area of interest [L^2], b is the thickness of the area of interest [L], and the other variables are as defined earlier. The gravitational force per area equals:

$$F_g = \frac{m * g}{A} = \frac{S_n * \rho_n * A * b * \Phi * g}{A} = S_n * \rho_n * b * \Phi * g \quad (22)$$

The gravitational force will increase linearly as the saturation of LNAPL increases.

4.2.3 Intermediate Wetting Phase Saturation

LNAPL is considered the intermediate wetting phase. The LNAPL saturation at any vertical position will be constant when the sum of the forces pulling the LNAPL up and the forces pulling the LNAPL down equal zero.

$$F_s - F_g = 0 \quad (23)$$

Substituting in for the two forces into Equation (23) allows for the average LNAPL saturation at any elevation to be found by solving for S_n .

$$S_c * \frac{\pi}{4*r} - S_n * \rho_n * b * \Phi * g = 0 \quad (24)$$

$$S_n = \frac{S_c * \frac{\pi}{4*r}}{\rho_n * b * \Phi * g} = \frac{S_c * \pi}{4*r * \rho_n * b * \Phi * g} \quad (25)$$

The thickness in the equation is unknown; however, we want to ensure the saturation changes with elevation. If we were to determine the thickness, it would be calculated as:

$$b = z - z_{datum} \quad (26)$$

where z is the elevation of interest [L] and z_{datum} is the elevation of the datum [L]. Setting the datum at the bottom of the LNAPL thickness would allow for $b = z$, and z would be positive.

Therefore, z will be substituted for b in Equation (25), resulting in:

$$S_n = \frac{S_c * \pi}{4*r * \rho_n * z * \Phi * g} \quad (27)$$

Equation (27) represents the LNAPL saturation if there were no water in the pores. Because it is assumed the media was originally water wet and the porosity is based on only air in the pores, the equation must be altered to account for residual water. This is accomplished by using an

effective porosity found by multiplying the measured porosity by $(1 - S_w)$, where S_w is the water saturation. The resulting equation is:

$$S_n = \frac{S_c * \pi}{4 * r * \rho_n * Z * \Phi * (1 - S_w) * g} \quad (28)$$

Equation (28) represents the intermediate wetting phase (LNAPL) saturation in a porous media. The value for the spreading coefficient in the LNAPL saturation equations was experimentally evaluated as well as compared to literature values. The spreading coefficient is based on a three-phase fluid system with the fluids being air, LNAPL, and water. The ring method, as defined in ASTM D971-12, was used to determine interfacial tensions. It was found that S_c is equal to 13.2 dyne/cm. The individual interfacial tensions measured were 72 dyne/cm for air-water, 28.3 dyne/cm for air-LNAPL, and 30.5 dyne/cm for LNAPL-water. These are similar to published values (ASTM D971-12; Bennett and Zisman, 1968; van Oss et al., 1992).

The value of the LNAPL spreading coefficient for a two-phase liquid system (the liquids being air and LNAPL) is defined differently. In this case, the interfacial tensions are based on the air-LNAPL-quartz system. This system has not been researched to the author's knowledge.

4.2.4 Wetting Phase Saturation

Water is considered the wetting phase. The water saturation can be evaluated the same way as the LNAPL saturation. Summing the spreading and gravity forces with respect to water results in the following equation for the wetting phase (water) saturation:

$$S_w = \frac{S_{cw} * \pi}{4 * r * \rho_w * Z * \Phi * g} \quad (29)$$

where S_{cw} is the spreading coefficient for water [M/L^2] and all other variables are as defined earlier. The water saturation can be defined in the same manner as the force balance for LNAPL because, once again, there are only the two forces acting on the water.

The spreading coefficient for water is dependent on the three phases in the system. For a three-phase liquid system (air, LNAPL, and water), the water spreading coefficient is based on the interfacial tensions of LNAPL-water-quartz. This value is not publicized to the author's knowledge. When evaluating the model for a three-phase liquid system, the water spreading coefficient was estimated at 25 dyne/cm.

The value of the water spreading coefficient for a two-phase liquid system (air and water) has been researched. The interfacial tensions are based on the air-water-quartz system. According to Jańczuk et al. (1984), the spreading coefficient for water can range from 89 dyne/cm to 118.2 dyne/cm. These values correspond to a contact angle of 0° and 53.2° , respectively. Since it is assumed that the water is completely wetting over the quartz, which correlates to an effective 0° contact angle, the spreading coefficient was deemed to be 89 dyne/cm.

4.2.5 Nonwetting Phase Saturation

Air is considered the nonwetting phase. The total saturation (all fluids) in a pore is 1 and equals the sum of the saturations of all individual elements.

$$S_t = 1 = S_{iw} + S_w + S_{nw} \quad (30)$$

where S is the saturation [dimensionless] and the subscripts t , iw , w , and nw represent the total, intermediate wetting phase (LNAPL), wetting phase (water), and nonwetting phase (air). The

intermediate and wetting phase saturations are defined in Equation (28) and (29), respectively. Rearranging Equation (30) the nonwetting phase (air) saturation can be found:

$$S_{nw} = 1 - S_{iw} - S_w \quad (31)$$

In a two-phase air-water system, the intermediate wetting phase saturation would be zero.

4.3 Comparison of Model and Data

After completing the derivation of the saturations for all three phases, the equations were compared to data (Figure 30). As can be seen in the graph, the data and model correlate poorly. The LNAPL and water saturations are under-predicted and the air saturation is over-predicted. The poor correlation suggests that the force balance model is incomplete. To determine what was missing, the author decided to simplify the situation to a two-phase system and verify the wetting phase saturation equation.

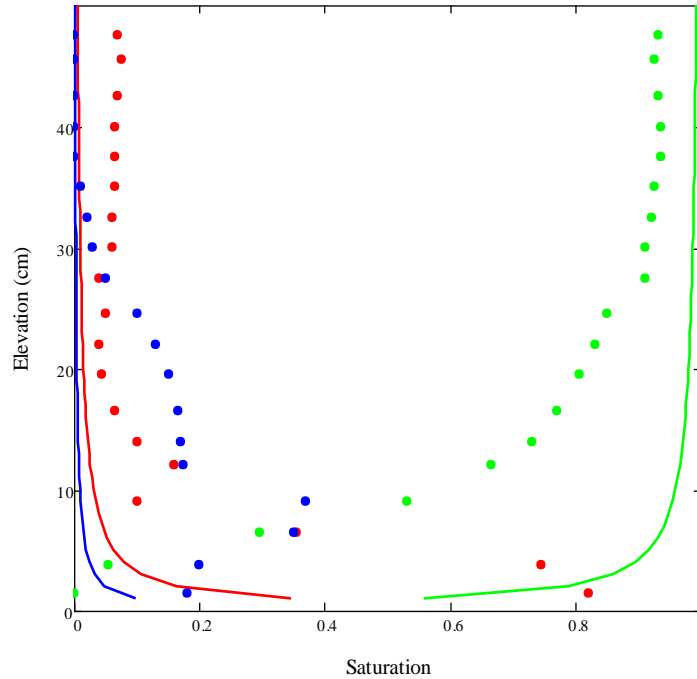


Figure 30. Data from Vizika and Lombard (1996) shown as dots compared to Model 1 shown as solid lines (green is air, red is LNAPL, and blue is water).

The wetting and nonwetting phase saturation equations from the model (herein referred to as Model 1) can be compared to data from Brooks and Corey (1964) and the Brooks-Corey equation. The data from Brooks and Corey (1964) uses LNAPL as the wetting phase instead of water. The spreading coefficient for this system (air-LNAPL-quartz) was not found in the literature. However, we can estimate the LNAPL spreading coefficient based on our knowledge of the water spreading coefficient in an air-water-quartz system. Like the water, the LNAPL is assumed to be completely coating the sand particles. However, $\sigma_{aw} > \sigma_{ao}$. Therefore, it was assumed that the LNAPL spreading coefficient would be less than the water spreading coefficient, which would be 89 dyne/cm. For this reason, a LNAPL spreading coefficient of 55 dyne/cm was used. The parameters of the porous media and for the Brooks-Corey equation are given in Table 6 (Section 4.2.1).

Figure 31 shows Model 1 compared to data for fine sand and the Brooks-Corey equation. The Brooks-Corey equation followed very closely to the data, however, the Model 1 line does not match. The Model 1 line needed to curve sharper in order to accurately depict the data. Model 2 in Figure 31 is an alteration to Model 1. Raising Equation (29) to a power allowed for the Model 1 line for the wetting phase saturation to curve more sharply, and follow the data more precisely. Following Brooks and Corey (1964) a power function, lambda, was employed. Graphing of the new model showed the curve was still slightly to the left of the data (not shown). The residual saturation was added to the new equation and S_w is redefined as follows:

$$S_w = \left(\frac{S_c * \pi}{4 * r * \rho_n * Z * \Phi * g} \right)^\lambda + S_r \quad (32)$$

Equation (32) represents Model 2, as shown in Figure 31. Note, the spreading coefficient and the density in the equation were changed to LNAPL values since LNAPL is the wetting phase. This line matched the Brooks-Corey equation almost exactly. Model 2 and the Brooks-Corey equation were compared for two other sets of media, volcanic sand and glass beads (Brooks and Corey, 1964). Throughout the three data sets, the λ value varied from 2.29 to 7.3. In each case, as long as the λ and S_r values were the same used in the Brooks-Corey equation, the models matched (Figure 32 and Figure 33).

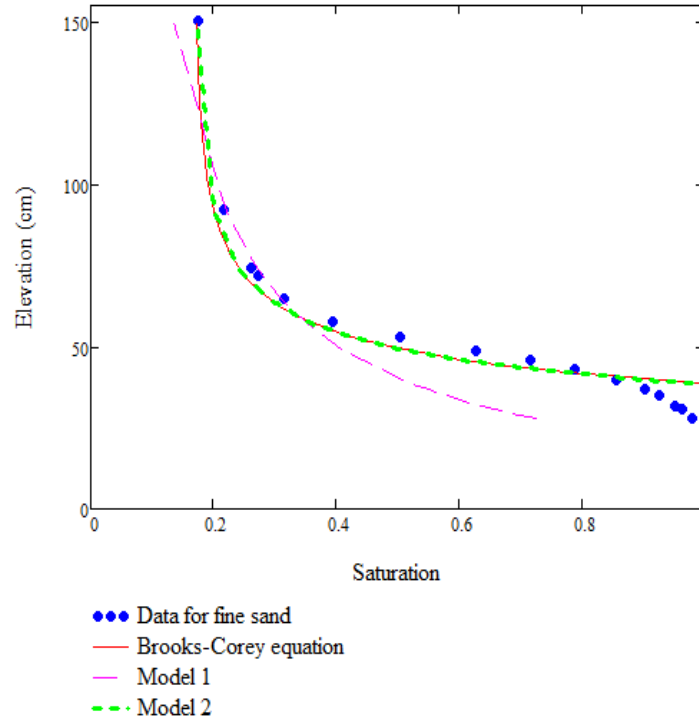


Figure 31. Graph depicting fine sand data (Brooks and Corey, 1964) and models.

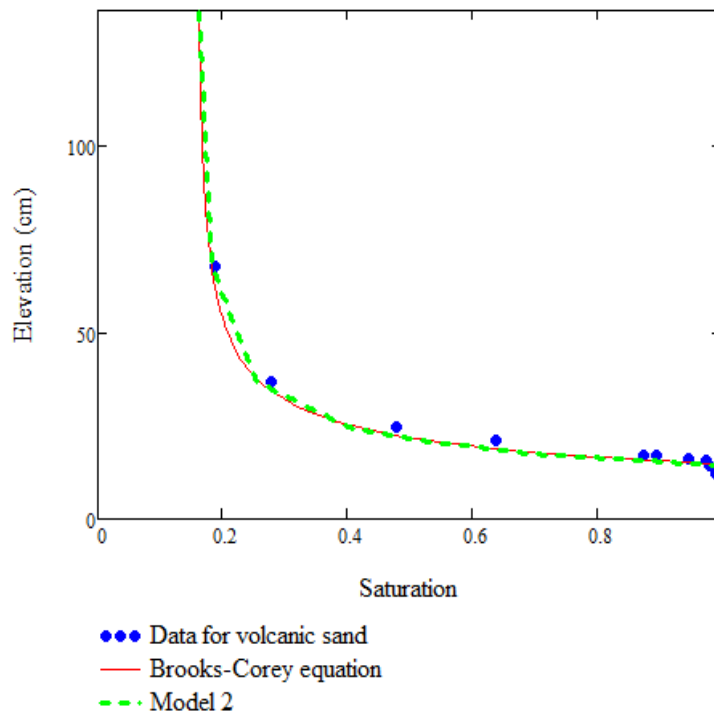


Figure 32. Graph depicting volcanic sand data (Brooks and Corey, 1964) and models.

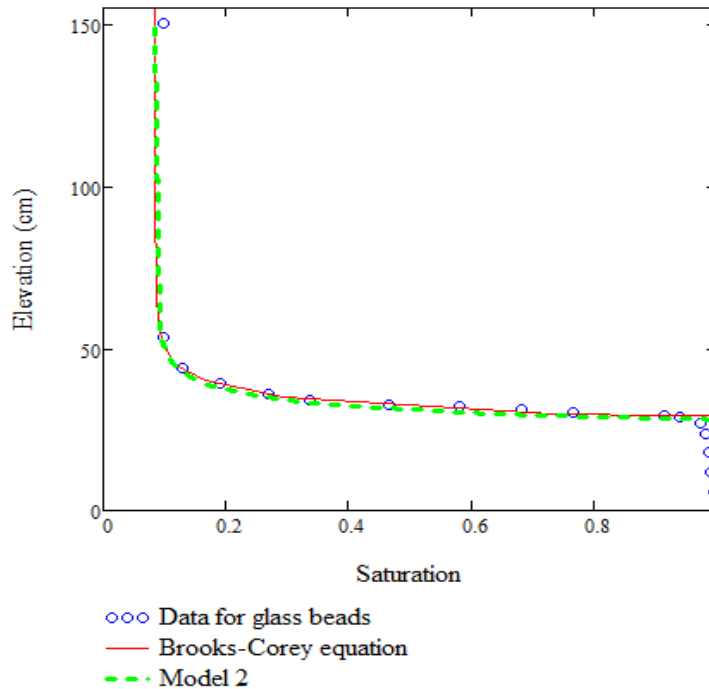


Figure 33. Graph depicting glass beads data (Brooks and Corey, 1964) and models.

Based on the fact that Model 2 matched the data and the Brooks-Corey equation for all three cases, it was observed that the model must be a power function and that λ is important. Lambda is the pore-size distribution index. Therefore, the sizes of pores within the media must be incorporated into the author's force balance approach model. More data and research needs to be performed to determine how λ fits into the force balance model and if it can be defined based on characteristics of the porous media and/or fluid.

A major limitation of the above results is the accuracy of the porous media radius for each set of data. Brooks and Corey (1964) does not specify the radius of the material used. The radius' used in the calculations were based on knowledge of average grain sizes for the media.

4.4 Conclusion

The model described in this chapter took a force balance approach to estimate fluid saturations versus elevation for a three-phase system. Model 1 was shown to be slightly off from the data in its calculations for fluid saturations. When looked at in a two-phase system, the wetting phase saturation was still low compared to the data. Model 1 was then altered to a power function using Brooks and Corey's λ variable and had the addition of the residual saturation. This new model, Model 2, matched the Brooks-Corey equation and data for multiple data sets. The possibility of being able to use a different ratio than the Brooks-Corey P_b/P_c to estimate saturation will be an excellent focus point of future research.

The comparison of the model to data suggests that there are more forces acting on the liquids than considered herein. The model also suggests that the pore-size distribution index plays an important role in determining the saturation of the wetting phase in a two-phase system.

Hopefully, the research presented here can be used as a basis to create an accurate force-based fluid saturation versus elevation model for a three-phase system.

5. CONCLUSION

Petroleum has been used for thousands of years and will continue to be used for the foreseeable future. Ongoing improvements of LNAPL management practices and remediation will assist in reducing LNAPL in subsurface settings and the formation of sheens at groundwater surface water interfaces. LNAPL migration towards GSIs is influenced by multiple processes.

Understanding where LNAPL is located, both geographically and within the subsurface, is imperative to managing further transport.

This chapter presents key results from this thesis and suggestions for future research.

5.1 Key Results

The first section of this thesis provided an overview of factors that affect the behavior of LNAPLs at GSIs. Key points of this section include:

- The use of fluorescent dyes can increase visualization of LNAPL contamination
- LNAPL occurrence in the subsurface can be broken into three distinct zones
 - Zone 1 occurs below the water capillary fringe where water is a continuous phase and LNAPL is a discontinuous phase. LNAPL migration is limited in this zone due to the occurrence of LNAPL as a discontinuous phase
 - Zone 2 occurs above Zone 1 and below the LNAPL capillary fringe where water and LNAPL are continuous phases. LNAPL migration is governed by Darcy's equations and occurs when $P_c > P_d$
 - Zone 3 occurs above the LNAPL capillary fringe where water, LNAPL, and air are continuous phases. LNAPL migration is governed by Darcy's equation

- LNAPL releases to surface water can be limited by reducing inflow ($LNAPL_{in}$), increasing storage capacity (REV_{cap}), enhanced losses ($LNAPL_D$), and/or recovery ($LNAPL_R$)
- Technological advances, and the use of fluorescent dyes, allowed for the creation of saturation curves based on photographs taken throughout the experiments

The second section of this thesis presented six laboratory sand tank experiments. The experiments provided insight into processes controlling LNAPL migration near GSIs. Key results include:

- Tidal cycles slow LNAPL migration by entrapping LNAPL in Zone 1 and smearing LNAPL in Zone 3
- LNAPL tends to migrate fastest in Zones 2 and 3 at low tide, when Zone 1 is minimized
- The volume of LNAPL in a well varies with water level fluctuations. The quantity is greatest at low water stages
- At vertical equilibrium, the quantity of LNAPL in a well can be related to the amount of LNAPL in Zone 2, but not the total LNAPL in the formation
- Vertical capillary barriers can limit lateral LNAPL migration. The processes to preclude migration depend on the zone
 - Zone 2 migration is limited due to the high displacement pressure of the fine media
 - Zone 3 migration is limited due to the high capillary rise within the barrier (speed bump)
- Recovery is a viable remediation technique and optimally should be performed at low tide, when there are increased thicknesses of LNAPL in the wells and Zone 2

- Organoclay barriers can have preferential pathways and slow drainage resulting in premature failure
- Simple modifications to organoclay barriers, such as impermeable baffles or coarse-grained drains, can improve performance
- Any containment system with constant inflow of LNAPL and no losses will ultimately fail

The third section of this thesis focuses on a force balance approach model to calculate fluid saturations versus elevation. Key results include:

- Current saturation models lack the spreading coefficient and contain fitting parameters
- A force balance model to determine LNAPL saturation is more complex than simply a spreading and gravity force
- By including lambda and residual saturation the model developed matches data and the Brooks-Corey model

The conclusions drawn from the work performed help reinforce information already known and advance ideas to improve remediation solutions for LNAPLs at GSIs.

5.2 Future Research

From the work presented here, the following research questions are proposed:

- Is there a relationship between particle size and how much LNAPL builds-up in front of a capillary barrier prior to overtopping/going under the barrier?
- Is there a prime location for the recovery well with respect to the barrier in order to maximize recovery?

- Do capillary barriers work equally well with other LNAPLs, such as benzene, toluene, ethylbenzene, and xylene?
- Do capillary barriers work with DNAPLs?
- Can other remedial techniques be employed in conjunction with a capillary barrier and recovery well to increase recovery/losses?
- Can geochemical conditions be modified in front of the capillary barrier to increase losses?
- What changes occur in hydraulic properties of an organoclay barrier when the organoclay is mixed with clay instead of sand? Does sorption increase when flux is reduced?
- Are there other, better options to modify organoclay barriers and increase sorption?
- Can microbes be introduced to an organoclay barrier to degrade LNAPL sorbed or are there byproducts that are created that reduce hydraulic conductivity?
- How do capillary and organoclay barriers perform in the field?

The following research is proposed regarding improvements on the Model 2:

- Collection of more two-phase data for comparison with Model 2, including actual grain size radii
- Determining if the use of λ and S_r can be used to calculate LNAPL saturations
- Determine how to define lambda in terms of the porous media and fluid properties
- Investigating more in-depth the similarities of the Brooks-Corey equation and Model 2
- Investigate the possibility of modifying the two-phase model for a three-phase system, including lambda and residual saturation
- The collection of more three-phase data for comparison

The above research would allow us to further understand 1) LNAPL migration, 2) the ability to prevent the formation of sheens, and 3) how to successfully choose an effective, sustainable, and low cost remedial solution. All of this is important to ensuring clean water, both surface and subsurface, for future generations.

6. REFERENCES

- American Petroleum Institute (API). 2002. Evaluating Hydrocarbon Removal from Source Zones and its Effect on Dissolved Plume Longevity and Magnitude. Washington, DC. API Publication 4715.
- ASTM International. 2012. Standard Test Method for Interfacial Tension of Oil Against Water by Ring Method. ASTM International, D971-12.
- Aubertin, M., E. Cifuentes, S. A. Apithy, B. Bussière, J. Molson, and R. P. Chapuis. 2009. Analyses of water diversion along inclined covers with capillary barrier effects. Canadian Geotechnical Journal, Vol. 46, pp. 1146-1164.
- Bernett, M. K. and W. A. Zisman. 1968. Effect of Adsorbed Water on Wetting Properties of Borosilicate Glass, Quartz, and Sapphire. Journal of Colloid and Interface Science, Vol. 29., No. 3, pp. 413-423.
- Blunt, M., D. Zhou, and D. Fenwick. 1995. Three-Phase Flow and Gravity Drainage in Porous Media. Transport in Porous Media, 20, pp. 77-103.
- Bright Solutions International, LLC. 2008. Material Safety Data Sheet BSL 715. Troy, MI.
- Brooks, R. H. and A. T. Corey. 1964. Hydraulic Properties of Porous Media. Hydrology Papers, Colorado State University, Fort Collins, CO.
- Burdine, N. T. 1952. Relative permeability calculations from pore-size distribution data. Trans. AIME, Vol. 146, pp. 107.

- Cary, J. W., C. S. Simmons, and J. F. McBride. 1989. Predicting Oil Infiltration and Redistribution in Unsaturated Soils. *Soil Sci. Soc. Am. J.*, 53, pp. 335-342.
- Chapman, S. W., B. L. Parker, T. C. Sale, and L. A. Doner. 2012. Testing high resolution numerical models for analysis of contaminant storage and release from low permeability zones. *Journal of Contaminant Hydrology*, 136-137, pp. 106-116.
- Charbeneau, R. J. 2000. *Groundwater Hydraulics and Pollutant Transport*. Prentice Hall, Upper Saddle River, NJ.
- Chatzis, I., A. Kantzas, and F. A. L. Dullien. 1988. On the investigation of gravity-assisted inert injection using micromodels, long Berea sandstone cores, and computer-assisted tomography. *Soc. Pet. Eng. Annual Technical Conference, Houston, TX, SPE-18284*. As cited by Hofstee et al., (1997).
- Corey, A. T. 1986. *Mechanics of Immiscible Fluids in Porous Media*. Water Resources Publication, Littleton, CO.
- Dwarkanath, V., R. E. Jackson, and G. A. Pope. 2002. Influence of Wettability on the Recovery of NAPLs from Alluvium. *Environmental Science and Technology*, 36, pp. 227-231.
- Farr, A. M., R. J. Houghtalen, and D. B. McWhorter. 1990. Volume Estimation of Light Nonaqueous Phase Liquids in Porous Media. *Groundwater*, Vol. 28, No. 1, pp. 48-56.
- Fraaije, J. G. E. M., and A. M. Cazabat. 1989. Dynamics of Spreading on a Liquid Substrate. *Journal of Colloid and Interface Science*, Vol. 133, No. 2, pp. 452-460.

- Gullick, R. W. and W. J. Weber Jr. 2001. Evaluation of Shale and Organoclays as Sorbent Additives for Low-Permeability Soil Containment Barriers. *Environmental Science and Technology*, 35, pp. 1523-1530.
- Hofstee, C., J. H. Dane, and W. E. Hill. 1997. Three-fluid retention in porous media involving water, PCE and air. *Journal of Contaminant Hydrology*, 25, pp. 235-247.
- Interstate Technology & Regulatory Council. 2009. Evaluating LNAPL Remedial Technologies for Achieving Project Goals. LNAPL-2. Washington, D.C.: Interstate Technology & Regulatory Council, LNAPLs Team. www.itrcweb.org.
- Jańczuk, B., E. Chibowski, and T. Białopiotrowicz. 1984. Time dependence wettability of quartz with water. *Chemistry Papers* 40 (3) pp. 349-356.
- Kalaydjian, F. and M. Tixier. 1991. Effect of the spreading coefficient on gas / oil capillary pressure curves in presence of connate water. Society of Core Analysis. Conf. paper No. 9106, presented at 5th SCA Annu. Tech. Conf., San Antonio, TX, Aug 20-22.
- Keller, A. A., M. J. Blunt, and P. V. Roberts. 1997. Micromodel Observation of the Role of Oil Layers in Three-Phase Flow. *Transport in Porous Media*. Vol. 26, pp. 277-297.
- Kemblowski, M. W. and C. Y. Chiang. 1990. Hydrocarbon Thickness Fluctuations in Monitoring Wells. *Groundwater*. Vol. 28, No. 2, pp. 244-252.
- Lee, S., A. H. Ören, C. H. Benson, and K. Dovantzis. 2012. Organoclays as Variably Permeable Reactive Barrier Media to Manage NAPLs in Ground Water. *Journal of Geotechnical and Geoenvironmental Engineering*, 138, pp. 115-127.

- Lenhard, R. J., J. C. Parker, and J. J. Kaluarachchi. 1989. A Model for Hysteretic Constitutive Relations Governing Multiphase Flow 3. Refinements and Numerical Simulations. *Water Resources Research*, Vol. 25, No. 7, pp. 1727-1736.
- Leverett, M. C. 1940. Capillary Behavior in Porous Solids. Tulsa Meeting, Petroleum Technology, pp. 152-169.
- Lo, E. M.-C. 2001. Organoclay with Soil-Bentonite Admixture as Waste Containment Barriers. *Journal of Environmental Engineering*, 127, pp. 756-759.
- Lo, I. M.-C. and Z. Yang. 2001a. Use of Organoclay as Secondary Containment for Gasoline Storage Tanks. *Journal of Environmental Engineering*, 127, pp. 154-161.
- Lo, I. M.-C. and Z. Yang. 2001b. Laboratory Investigation of the Migration of Hydrocarbons in Organobentonite. *Environmental Science and Technology*, 35, pp. 620-625.
- Mahler, N., T. Sale, T. Smith, and M. Lyverse. 2011. Use of Single-Well Tracer Dilution Tests to Evaluate LNAPL Flux at Seven Field Sites. *Groundwater*, NGWA.org.
- Marinelli F. and D. S. Durnford. 1996. LNAPL Thickness in Monitoring Wells Considering Hysteresis and Entrapment. *Groundwater*, Vol. 34, No. 3, pp. 405-414.
- McBride, J. F., C. S. Simmons, and J. W. Cary. 1992. Interfacial spreading effects on one-dimensional organic liquid imbibition in water-wetted porous media. *Journal of Contaminant Hydrology*, 11, pp. 1-25.
- McCartney, J. S. and J. G. Zornberg. 2010. Effects of infiltration and evaporation on geosynthetic capillary barrier performance. *Canadian Geotechnical Journal*, Vol. 47, pp. 1201-1213.

- Mercer, J. W. and R. M. Cohen. 1990. A Review of Immiscible Fluids in the Subsurface: Properties, Models, Characterization and Remediation. *Journal of Contaminant Hydrology*, 6, pp. 107-163.
- Morrow, N. R. and G. Mason. 2001. Recovery of oil by spontaneous imbibition. *Current Opinion in Colloid & Interface Science*, 6, pp. 321-337.
- Mualem, Y. 1976. A new model for predicting the hydraulic conductivity of unsaturated porous media. *Water Resources Research*, Vol. 12, pp. 513-522.
- The New Encyclopædia Britannica. 2005. Fossil Fuels. *The New Encyclopædia Britannica*, 15th Edition, Chicago, IL.
- Oostrom, M., C. Hofstee, R. J. Lenhard, and T. W. Wietsma. 2003. Flow behavior and residual saturation formation of liquid carbon tetrachloride in unsaturated heterogeneous porous media. *Journal of Contaminant Hydrology*, 64, pp. 93-112.
- Padday, J.F. 1992. Spreading, wetting, and contact angles. *Journal of Adhesion Science Technology*, Vol. 6, No. 12, pp. 1347-1358.
- Pantazidou, M. and N. Sitar. 1993. Emplacement of Nonaqueous Liquids in the Vadose Zone. *Water Resources Research*. Vol. 29, No. 3, pp. 705-722.
- Parent, S.-E. and A. Cabral. 2005. Material Selection for the Design of Inclined Covers with Capillary Barrier Effect. *Waste Containment and Remediation*, GSP 142.
- Parker, J. C. and R. J. Lenhard. 1987. A Model for Hysteretic Constitutive Relations Governing Multiphase Flow 1. Saturation-Pressure Relations. *Water Resources Research*, Vol. 23, No. 12, pp. 2187-2196.

- Parker, J. C. 1989. Multiphase Flow and Transport in Porous Media. *Review of Geophysics*, Vol. 27, No. 3 pp. 311-328.
- Qian, T., L. Huo, and D. Zhao. 2009. Laboratory Investigation into Factors Affecting Performance of Capillary Barrier System in Unsaturated Soil. *Water Air Soil Pollution*, Vol. 206, pp. 295-306.
- Sale, T. and D. Applegate. 1997. Mobile NAPL Recovery: Conceptual, Field, and Mathematical Considerations. *Groundwater*. Vol. 35, No. 3, pp. 418-426.
- Sale, T., G. R. Taylor, G. Iltis, and M. Lyverse. 2007. Measurement of LNAPL Flow Using Single-Well Tracer Dilution Techniques. *Groundwater*, Vol. 45, No. 5, pp. 569-578.
- San Joaquin Valley Geology. 2011. http://www.sjvgeology.org/history/gushers_world.html
- Schroth, M. H., J. D. Istok, S. J. Ahearn, and J. S. Selker. 1995. Geometry and position of light nonaqueous-phase liquid lenses in water-wetted porous media. *Journal of Contaminant Hydrology*, 19, pp. 269-287.
- Sciencelab.com, Inc. 2005. Material Safety Data Sheet Fluorescein Sodium. Houston, Texas. Sciencelab.com.
- Schwille, F. 1988. *Dense Chlorinated Solvents in Porous and Fractured Media*. Second Edition. Lewis Publishers. Chelsea, Michigan.
- Shackelford, C. D., C.K- Chang, and T.-F. Chiu. 1994. The Capillary Barrier Effect in Unsaturated Flow Through Soil Barriers. *Proceedings of the First International Congress on Environmental Geotechnics*.

Spectronics Corporation. 2010. Material Safety Data Sheet OIL-GLO™. Westbury, New York.

U.S. Energy Information Administration. 2012. U.S. Crude Oil Supply & Disposition.

<http://205.254.135.7/petroleum/>

U.S. Environmental Protection Agency. 1989. Requirements for hazardous waste landfill design, construction, and closure. *EPA/625/4-89/022*, Cincinnati.

U.S. Environmental Protection Agency. 1998. Technical Protocol for Evaluating Natural Attenuation of Chlorinated Solvents in Ground Water. Office of Research and Development. Washington D.C.

U.S. Environmental Protection Agency. 2011. National Pollutant Discharge Elimination System (NPDES): Clean Water Act. cfpub.epa.gov/npdes/cwa.cfm?program_id=6.

U.S. Environmental Protection Agency. 2012. Introduction to the Clean Water Act. Watershed Academy Web. cfpub.epa.gov/watertrain/moduleFrame.cfm?parent_object_id=2571.

van Genuchten, R. T. 1980. A Closed-form Equation for Predicting the Hydraulic Conductivity of Unsaturated Soils. *Soil Sci. Soc. Am. J.*, 44, pp.892-898.

van Oss, C. J., R. F. Giese, Z. Li, K. Murphy, J. Norris, M. K. Chaudhury, and R. J. Good. 1992. Determination of contact angles and pore sizes of porous media by column and thin layer wicking. *Journal of Adhesion Science and Technology*, Vol. 6, No. 4, pp. 413-428.

Vizika, O. and J. M. Lombard. 1996. Wettability and Spreading: Two Key Parameters in Oil Recovery with Three-Phase Gravity Drainage. *SPE Reservoir Engineering*. February.

Voudrias, E. A. 2002. The concept of a sorption chemical barrier for improving effectiveness of landfill liners. *Waste Management and Research*, 20, pp. 251-258.

Wilson, J. L., S. H. Conrad, W. R. Mason, W. Peplinski, and E. Hagan. 1990. Laboratory Investigations of Residual Liquid Organics from Spills, Leaks, and the Disposal of Hazardous Wastes in Groundwater. EPA/600/6-90/004.

Young, T. 1805. An Essay on the Cohesion of Fluids. *Phil. Trans. R. Soc. London*, 95, pp.65-87.

Zornberg, J. G., A. Bouazza, and J. S. McCartney. 2010. Geosynthetic capillary barriers: current state of knowledge. *Geosynthetics International*, Vol. 17, No. 5, pp. 273-300.

7. APPENDIX A

```
% Saturation Curve
RGB=imread('PICTURE OF INTEREST.jpg');
% decimal in below formula is luminescence level that must be changed for
% each picture
BW=im2bw(RGB,0.3);
% pixheight is height of picture in pixels, pixwidth is width of picture in
% pixels
pixheight=1735
pixwidth=2314
% hpic is the actual size in cm of the picture
hpic=25
height=(1:pixheight);
for ii=1:pixheight;
    slicelumin(ii)=mean2(BW(ii:ii+1,1:end));
end;
figure, plot(slicelumin(height), (pixheight-height)*hpic/pixheight);
xlabel('Saturation'); ylabel('Distance from low tide (cm)');
title('Saturation Curve');
figure, imshow(BW);
AUC2=sum(sum(BW));
% AUC is the sum of all white pixels
avesat=AUC2/((pixheight+1)*pixwidth)
```

8. SUPPLEMENTAL MATERIAL

Three videos of the experiments are available for view. The first video focuses on capillary barriers and the ability to remove LNAPL from the formation. The second video looks at the first organoclay barrier experiment containing a simple organoclay barrier. The third video captures the improved organoclay barriers, baffles and drains. All three videos can be found on the website for the Center for Contaminant Hydrology at Colorado State University. The web address is <http://www.engr.colostate.edu/CCH/research.shtml>. The following are narratives that accompany each video.

8.1 Capillary Barrier Video

As the video begins, you will see two pictures. The one in the upper right is a zoomed out picture of the tank, and the main picture is zoomed in to the area of interest. As the LNAPL first hits the barrier, you can see that it is unable to penetrate the barrier. The capillary rise in the barrier prevents Zone 3 LNAPL from flowing over the barrier, and the LNAPL cannot build up enough capillary pressure to overcome the displacement pressure in Zone 2.

As we continued to add LNAPL, it continues to build-up in Zone 2 in the tank. Even though 3.3 L of LNAPL was fed in to the tank, the barrier prevents the LNAPL from further migration. The LNAPL does not reach a high enough capillary pressure to overcome the displacement pressure. When the barrier fails, you can see it is because the LNAPL actually goes under the barrier due to limitations of the tank. This experiment led to the question, how much LNAPL can be removed from the tank?

Another experiment was performed, similar to the first, with the exception that the next experiment has two wells present. Two and a half liters of LNAPL were added to the tank for

this experiment. You can see that the amount of LNAPL in the well changes with the tide; there is more LNAPL in the well at low tide than at high tide. You can also see that the amount of LNAPL in the well does not correlate with the amount of LNAPL in the formation.

After the 2.5 L were added, we began to pump LNAPL out of the tank and did so at low tide. You will notice at every other low tide the amount of LNAPL in the well jumps and this is when we are pumping. Overall, we were able to recover 92% of the LNAPL originally fed into the tank. This is a large amount recovered and was more than expected. Granted, this is a homogeneous isotropic media and not necessarily representative of field conditions.

8.2 Organoclay Barrier Video

This video is set up the same as the capillary video with a picture on picture. As the LNAPL first hits the barrier, it is prevented from entering the barrier. The organoclay looks as though it is initially acting as a capillary barrier. The LNAPL in Zone 2 does not have a high enough capillary pressure to enter into the barrier and slow drainage prevents LNAPL in Zone 3 from entering the barrier. Although it initially looks to hold back the LNAPL, we soon see overtopping and preferential flow paths become issues.

Because the barrier is hydrophobic, the top pores are not full of water. As the LNAPL builds up enough thickness in Zone 2, it is able to overtop the barrier and flow across the top of the barrier. As the barrier then drains with the tide, the LNAPL is able to create preferential flow paths. The slow drainage that you can faintly see is the reason that the LNAPL cannot enter the barrier from the side.

As more LNAPL is added, preferential flow continues to be an issue. What we would like to see is the LNAPL enter through the side which begins to happen just prior to failure. The preferential flow issues ultimately led to the barrier's early failure.

8.3 Improved Organoclay Barrier Video

This video shows the organoclay barrier experiment with baffles and coarse-grained drains. We will first look at the organoclay barrier with three HDPE baffles. As the LNAPL first enters the barrier it looks as though the LNAPL still overtops through the first baffle, but this is just an imperfection between the baffle and the glass wall of the tank. As we continue to add LNAPL you can see that the LNAPL is moving in from the side and travelling through the barrier. Already you can see a larger amount of LNAPL has sorbed to the organoclay prior to failure.

The second barrier has coarse sand acting as drains. At low tide the LNAPL goes under the organoclay portions. The coarse sand acts as a new preferential flow path. At the same time though, the organoclay is draining better and allowing the LNAPL to make contact with the organoclay and sorb. The barrier fails due to the newly created preferential flow path in the coarse sand and under the organoclay.

Both of these improved organoclay barriers have higher sorption, but there is still room for improvement.